

# Fundamentals of GISANS and Selected Examples



Johannes Schlipf,  
Peter Müller-Buschbaum

Technische Universität München  
Lehrstuhl für Funktionelle Materialien  
Physik-Department  
James-Franck-Str. 1  
85748 Garching b. München  
Germany



# Outline

- Fundamental Aspects of GISANS
- Selected Examples
- Monitoring the Ingression of Moisture into Hybrid Perovskite Thin Films with In-Situ GISANS

+ ACS LiveSlides  
video





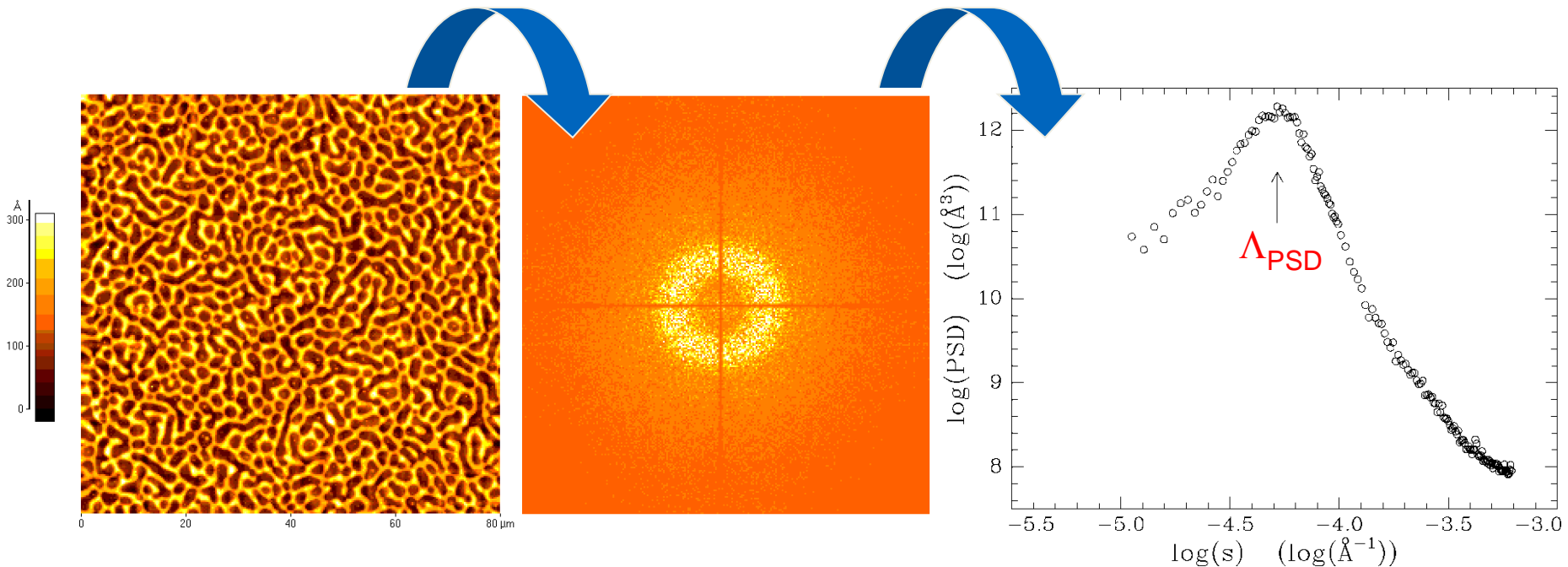


German Black Forest Cherry Cake

looking for a more non-destructive way ...

# Statistical analysis of AFM data

isotropic structure  $\rightarrow$  circular ring  $\rightarrow$  well described by one in-plane length

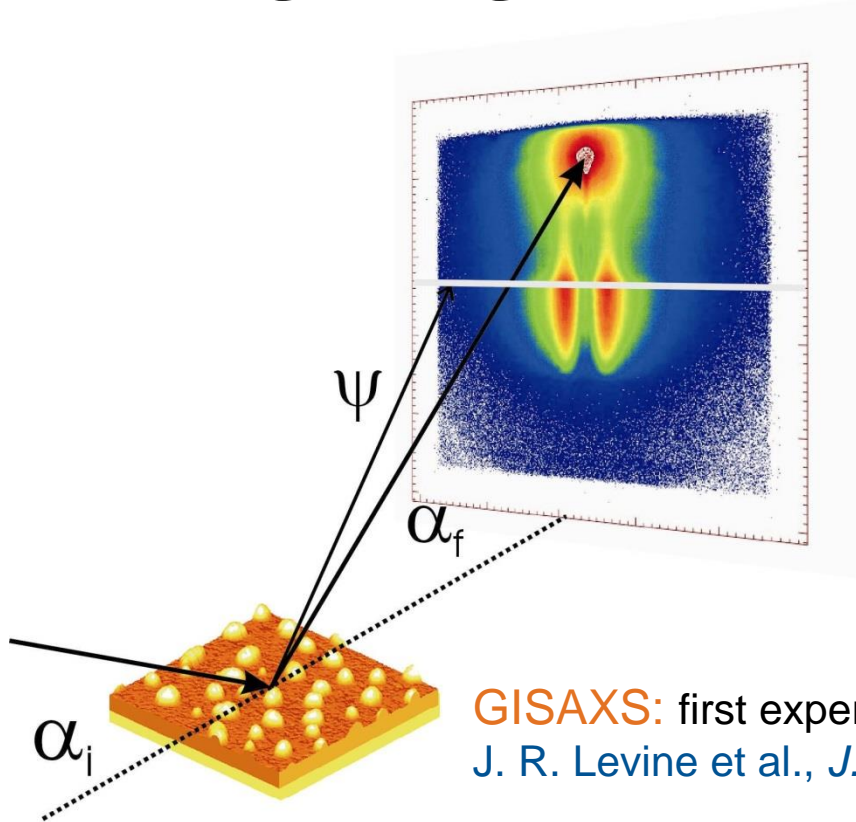


AFM data accessible with scan ranges up to  $\approx 100 \mu\text{m}$

$\rightarrow$  determination of most prominent in-plane length  $\Lambda_{\text{PSD}}$

$\rightarrow$  only sample surface probed !

# GISAS (grazing incidence small angle scattering)



- fixed incidence angle  $\alpha_i \ll 1^\circ$
- two high quality entrance cross-slits
- mostly evacuated pathway
- two dimensional detector array
- controlling sample position and orientation with respect to the beam

**sample-detector distance  
determines resolution**  
→ **sub-nm up to several  $\mu\text{m}$**

**GISAXS:** first experiment:  
J. R. Levine et al., *J. Appl. Cryst.* **1989**, 22, 528

**GISANS:**  
P. Müller-Buschbaum et al., *Colloid. Polym. Sci.* **1999**, 277, 1193

**Reviews:** P. Müller-Buschbaum, *Polymer Journal* **2013**, 45, 34

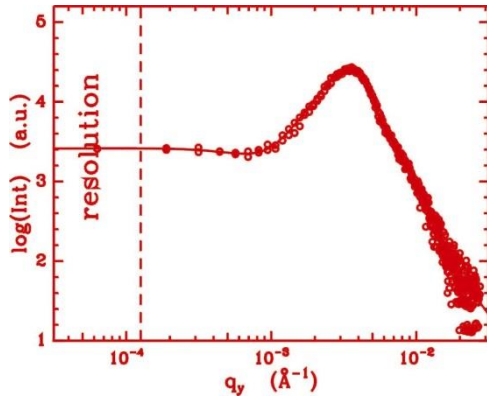
P. Müller-Buschbaum, *European Polymer Journal* **2016**, 81, 470





# Line cuts

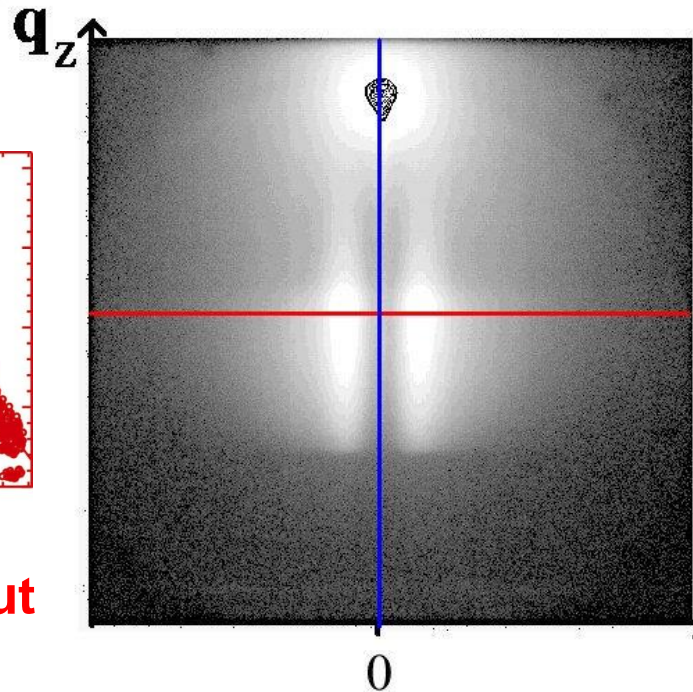
cut at constant  $q_z$



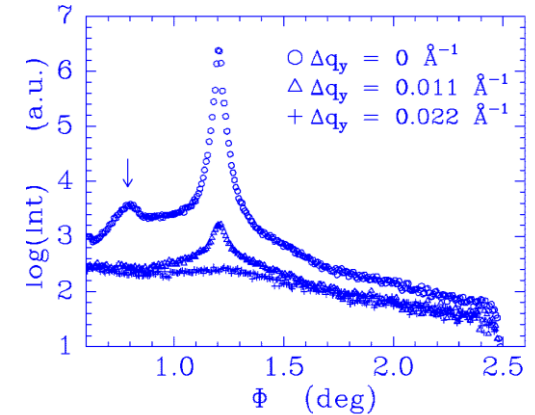
**horizontal line cut**

→  $q_y$ -dependence:  
 in-plane structures

distorted wave  
 Born approximation  
 (DWBA)

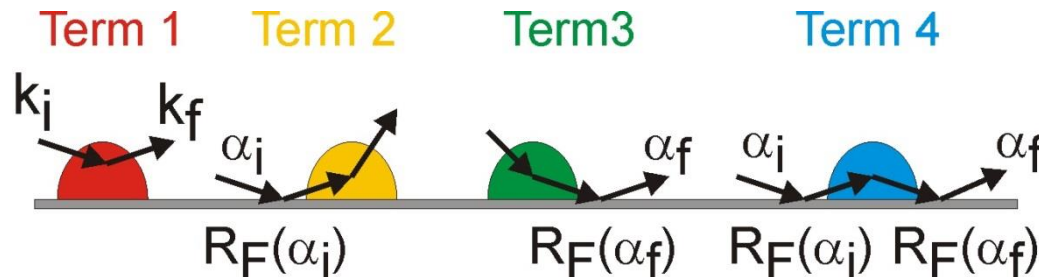


cut at constant  $q_y$



**vertical line cut**

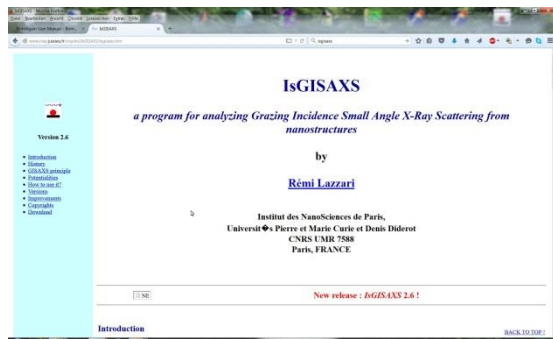
→ mainly  $q_z$ -dependence:  
 correlation perpendicular  
 to surface



# Modelling of GISANS data

## several software packages

### IsGISAXS



R. Lazzari, *J. Appl. Cryst.* **2002**, 35, 406

### FitGISAXS



D. Babonneau, *J. Appl. Cryst.* **2010**, 43, 929

### HipGISAXS



S. Chourou et al., *J. Appl. Cryst.* **2013**, 46, 1781

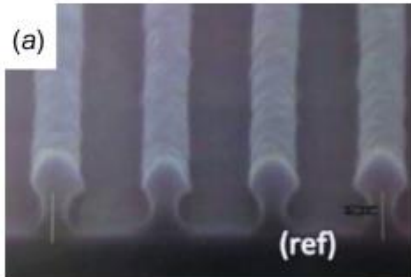
### BornAgain



→ [bornagainproject.org](http://bornagainproject.org)

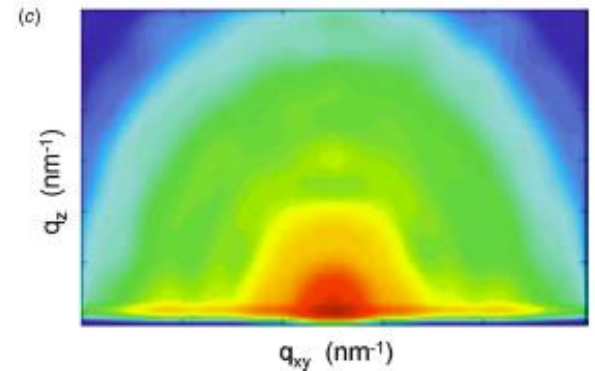
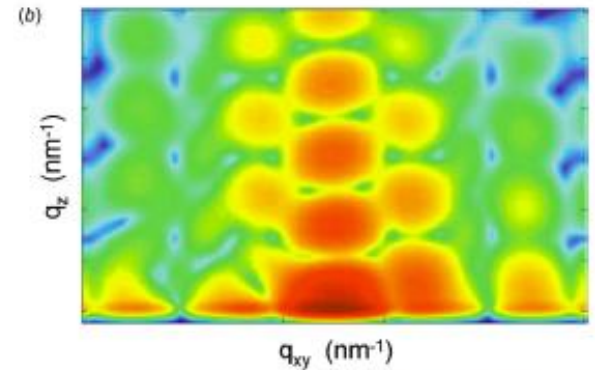
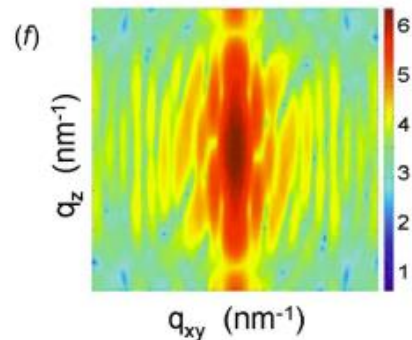
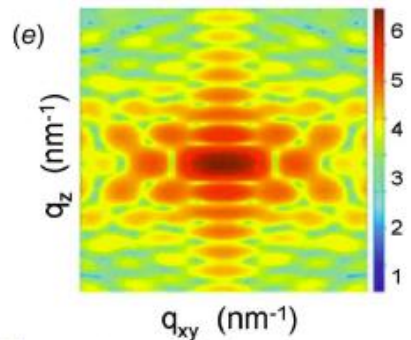
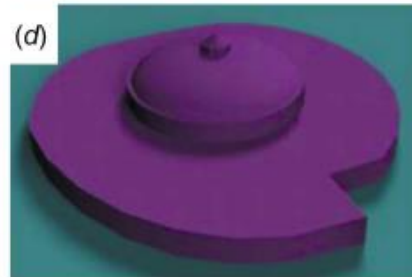
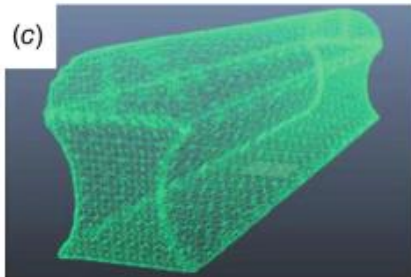
# Modelling of complex samples

both for x-rays and neutrons



HipGISAXS  
from ALS

S. Chourou et al.,  
*J. Appl. Cryst.*  
**2013**, 46, 1781

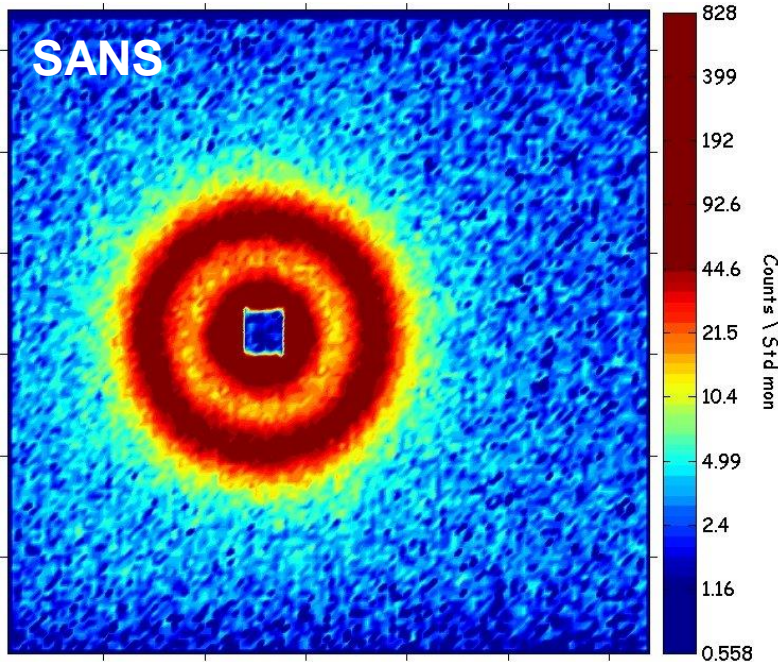


A. Hexemer, P. Müller-Buschbaum, *IUCrJ* **2015**, 2, 106-125



# Comparison SANS versus GISANS

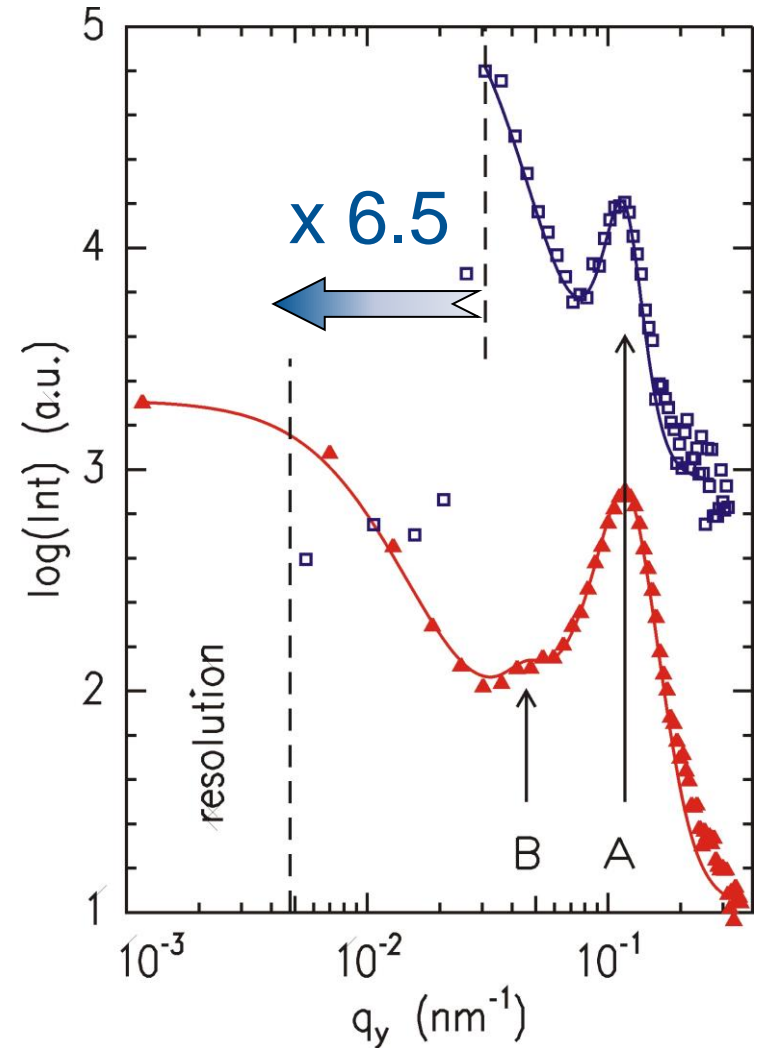
thick tri-block copolymer film



SANS and GISANS yield lamellar spacing  $L_0 = \Lambda_A = 47$  nm

GISANS has higher resolution  
 → second length  $\Lambda_B = 300$  nm

P. Müller-Buschbaum et al., *Langmuir* **2006**, *22*, 9295

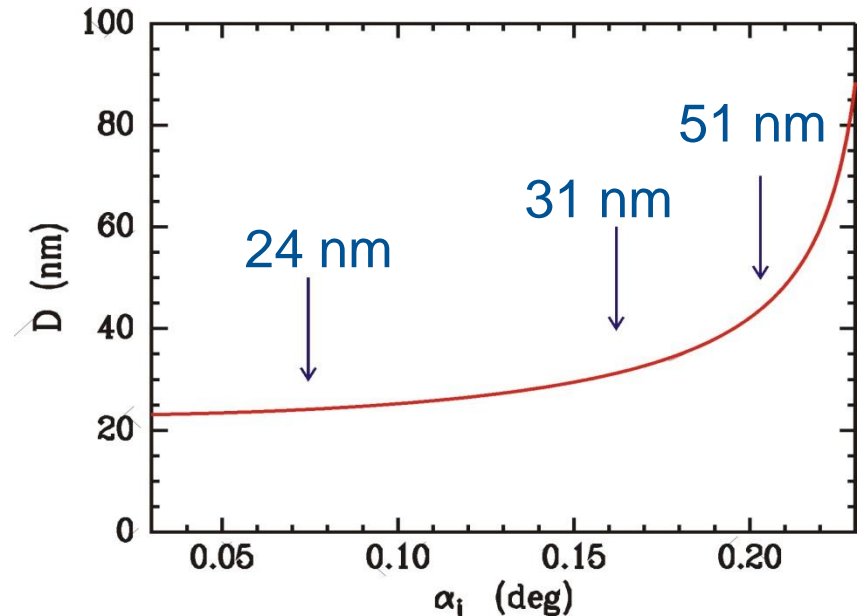
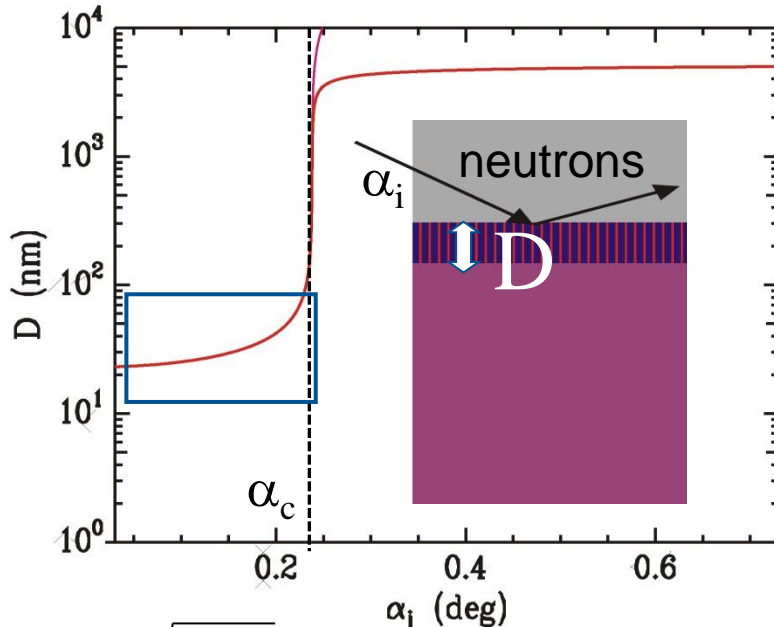


# Surface sensitivity

scattering depth of neutrons

$$D = \frac{\lambda}{\sqrt{2\pi}(l_i + l_f)}$$

$$l_{i,f} = \left[ \sin^2 \alpha_c - \sin^2 \alpha_{i,f} + \sqrt{(\sin^2 \alpha_{i,f} - \sin^2 \alpha_c)^2 + \left(\frac{\mu\lambda}{2\pi}\right)^2} \right]^{1/2}$$



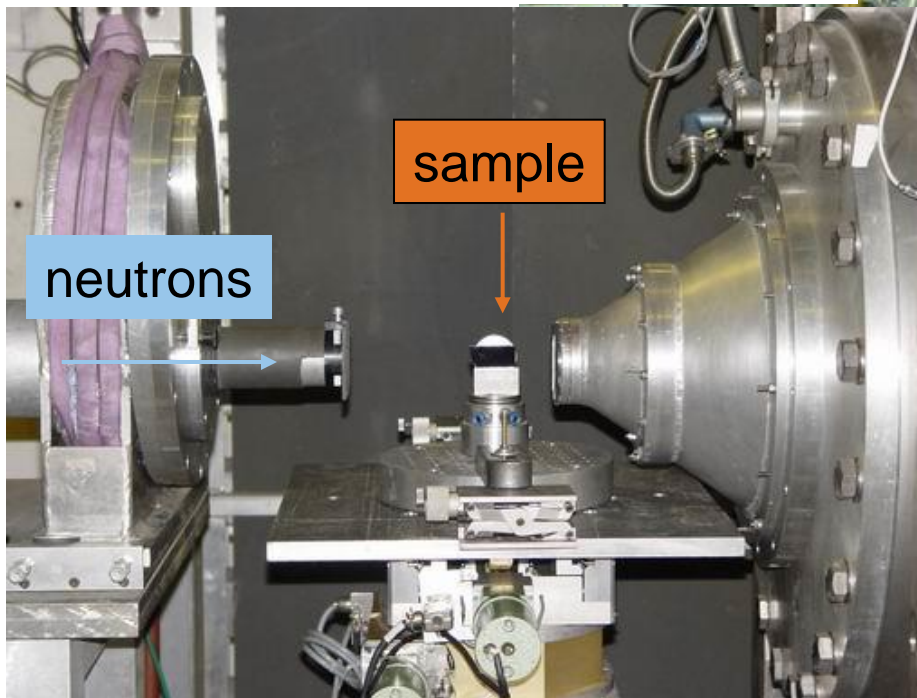
$$\alpha_c = \lambda \sqrt{\frac{\rho_{SLD}}{\pi}} \rightarrow \text{vary incident angle } \alpha_i < \alpha_c \text{ to probe interface near region}$$

# GISANS at D22

with R. Cubitt

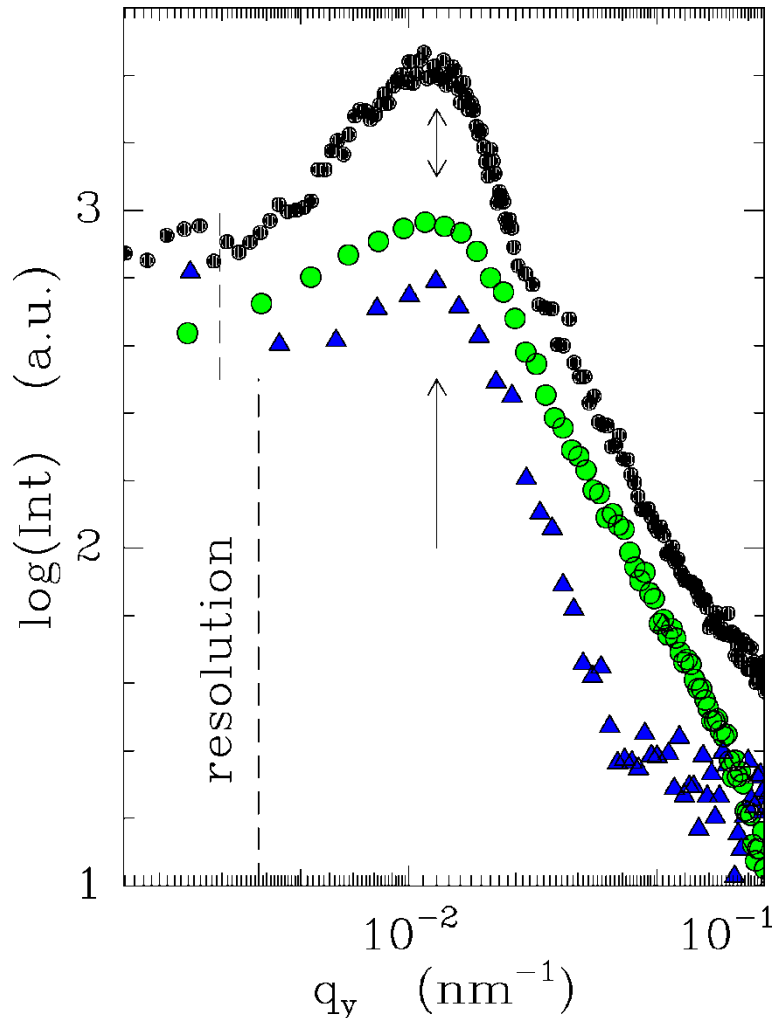
sample--detector distance 17.6 m  
collimation length 17.6 m

slit  $1 \times 10 \text{ mm}^2$





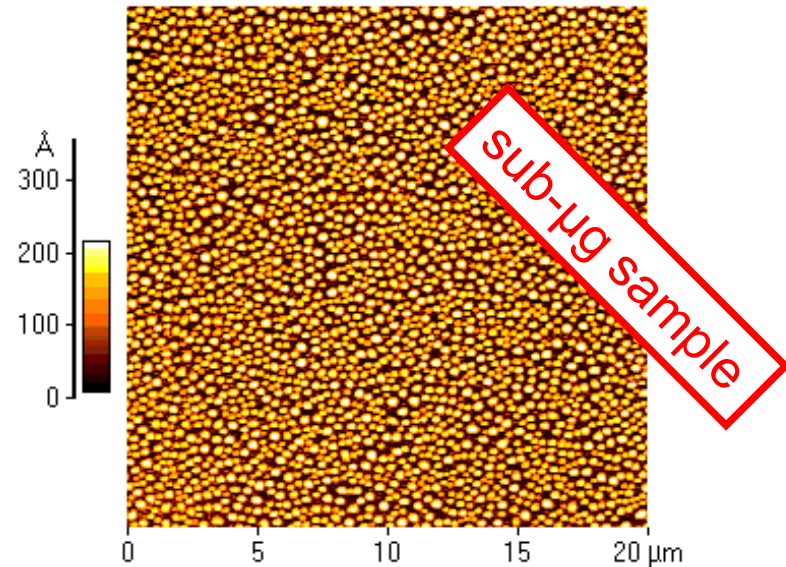
# Polymer nano-droplets



dPS on Si/SiO<sub>x</sub>

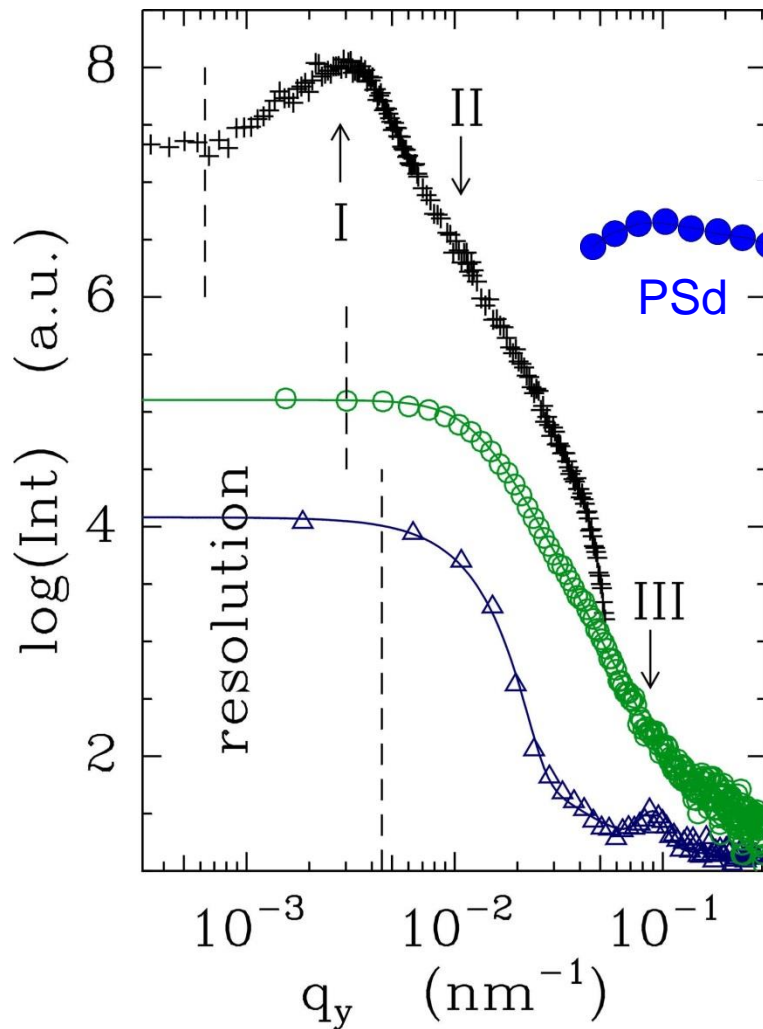
$h < 1/3 R_g$

toluene vapor treatment



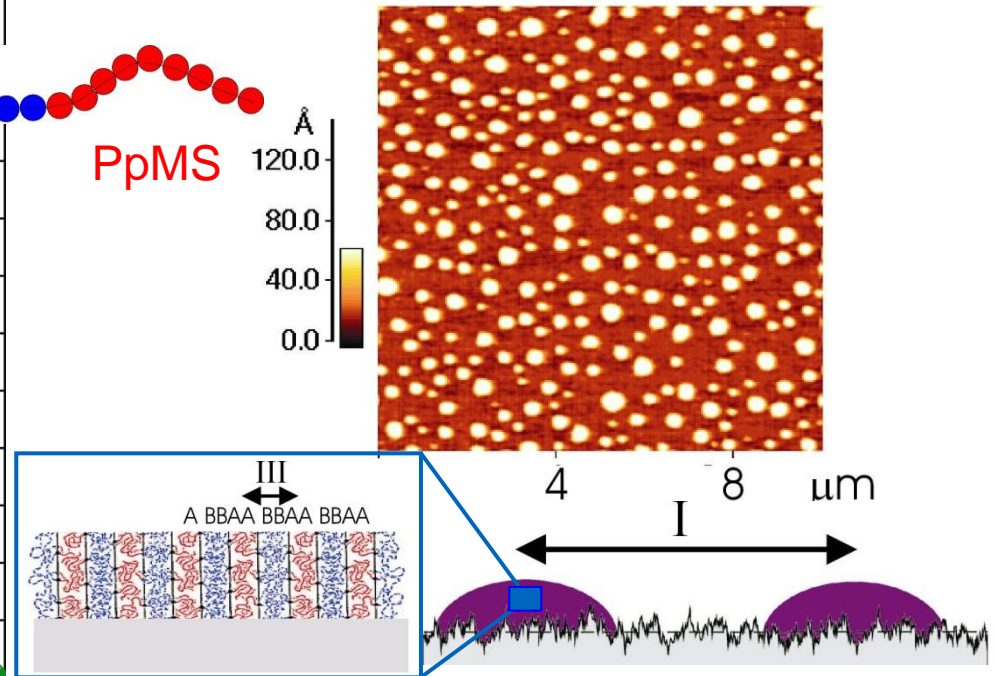
**small droplets:** prominent in-plane  
 length scale of  $\Lambda_t = 522 \pm 5$  nm  
 → well pronounced peak in **GISAXS**  
 and **GISANS** or in **AFM** data

# Internal nano-structure



P(Sd-b-pMS) on Si/SiO<sub>x</sub>  $h < 1/3 R_g$

toluene vapor treatment 12h



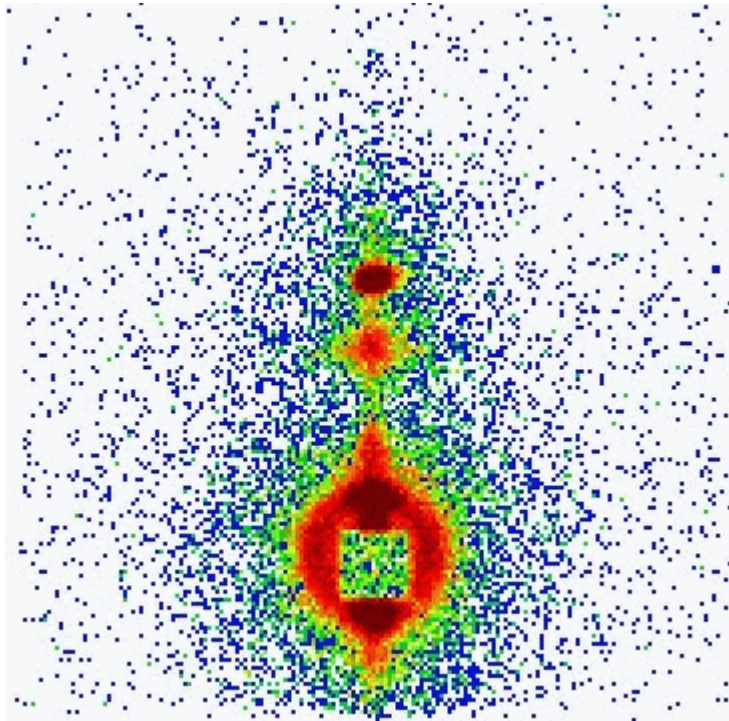
large drops (I) only resolved by **AFM**  
 small structure (III) only visible with **GISANS** not with **GISAXS**

# TOF-GISANS at REFSANS

48 h counting time, using 5 beams

sample-detector distance 10.7 m

wavelength range 0.25 – 1.49 nm



- select region of interest from 2D intensity
- TOF superposition of many wavelengths
- definition of individual time channels

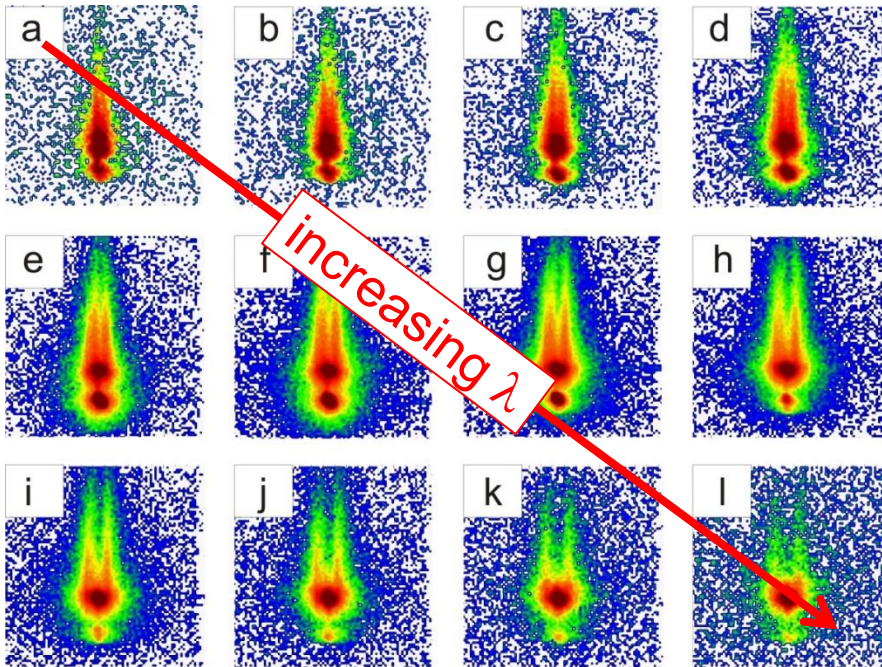


# Polymer nano-droplets

dPS on top of Si/SiO<sub>x</sub>

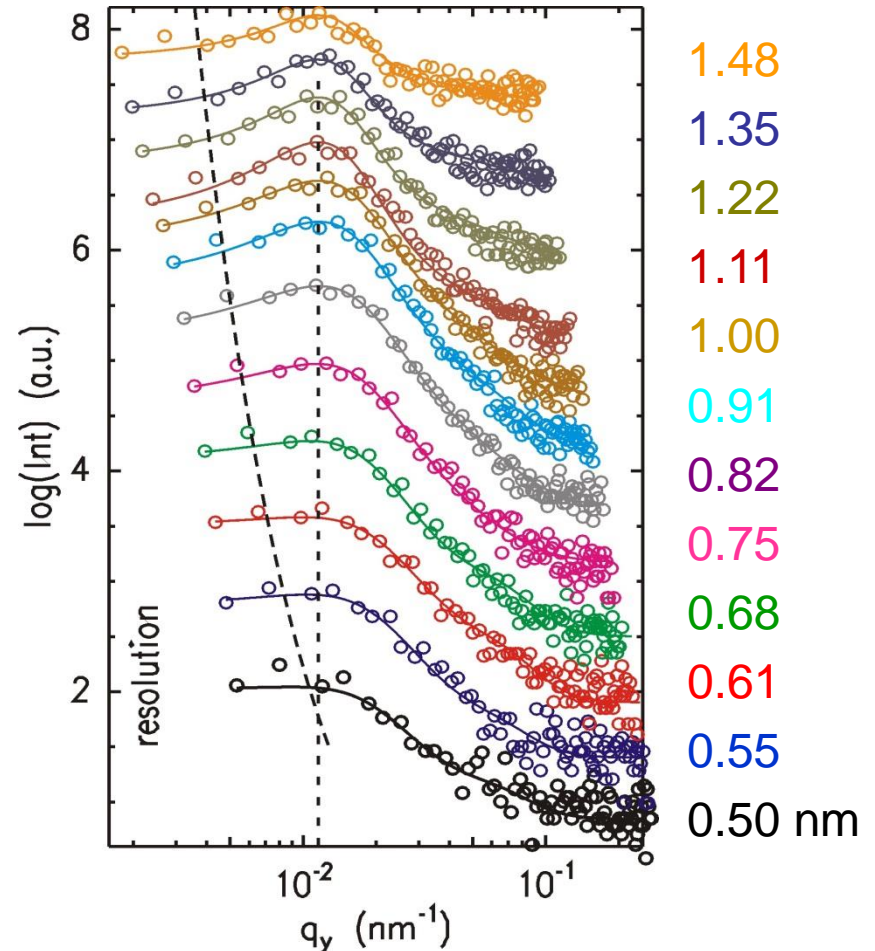
$h < 1/3 R_g$

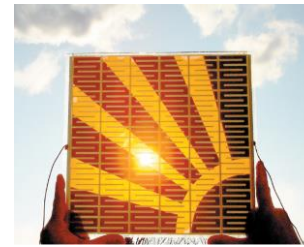
toluene vapor treatment



structure factor of droplet assembly  
 well resolved

$$\alpha_c = \lambda \sqrt{\frac{Nb}{\pi}}$$

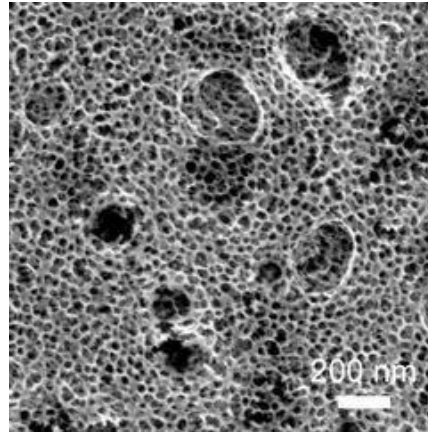
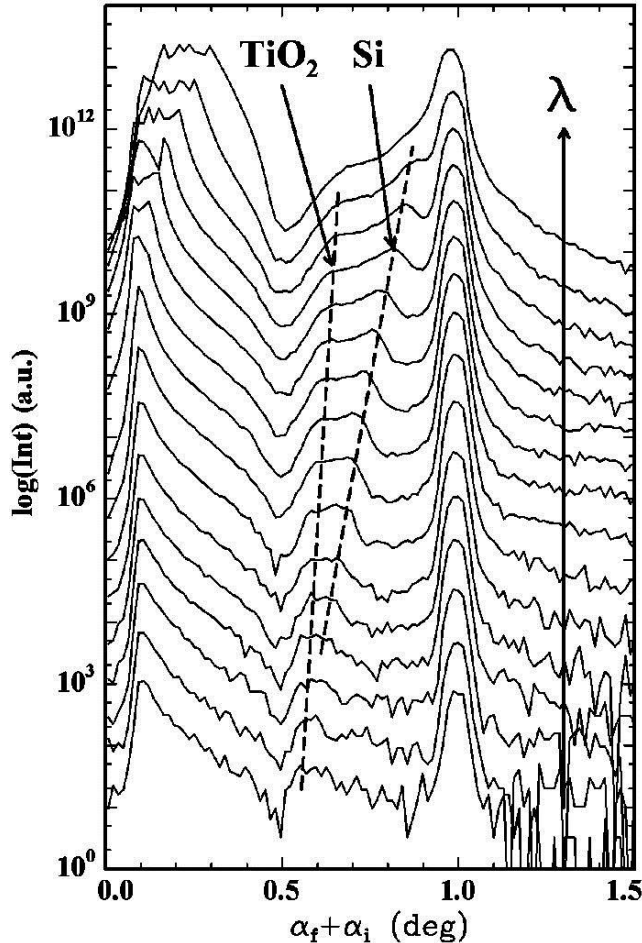




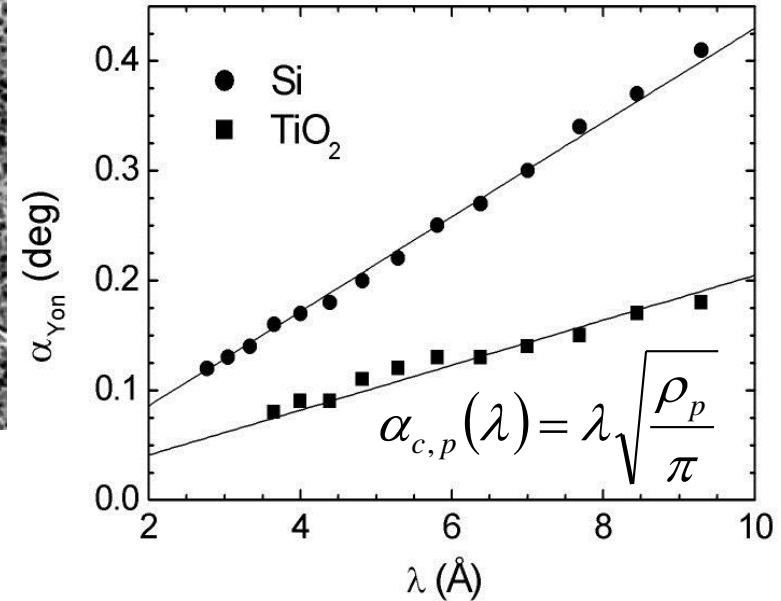
icis.com

# Porosity determination

**TOF-GISANS:** vertical cuts → extract Yoneda peak positions

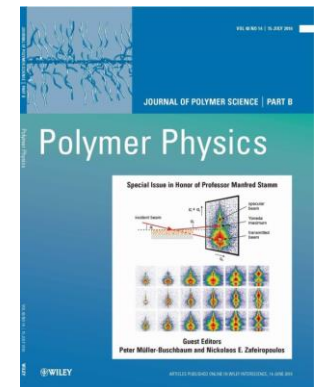


TiO<sub>2</sub> sponge-like morphology



→ porosity of 85%

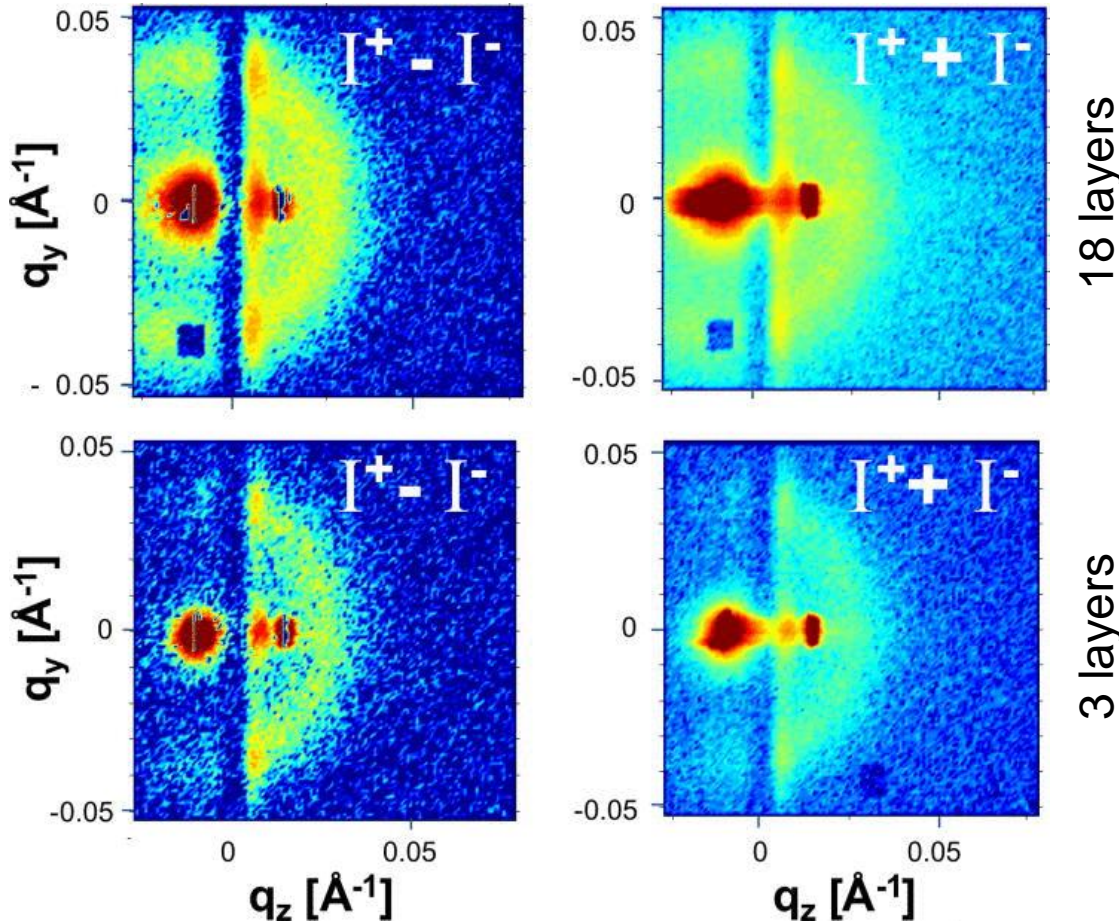
access to quantitative porosity of film





# Polarized GISANS

Co nanoparticles on Si/SiO<sub>x</sub> at fields of 110 mT



D22, data taken with spin flipper in front of sample

Debye-Scherrer rings with strong magnetic contrast  
 → short range lateral order of 13 nm nanoparticles with  $\Lambda = 17$  nm



# Summary

**GISANS opens new possibilities of advanced sample characterization**

**GISAS : reciprocal space analysis technique**

- *non-destructive structural probe*
- sensitive to structures between 1 nm to 5 (or 21)  $\mu\text{m}$
- does not require a special sample preparation
- *yields excellent sampling statistics*  
(averages over macroscopic regions to provide information on nanometer scale)



- **buried structures:** object geometry, size distributions and spatial correlations

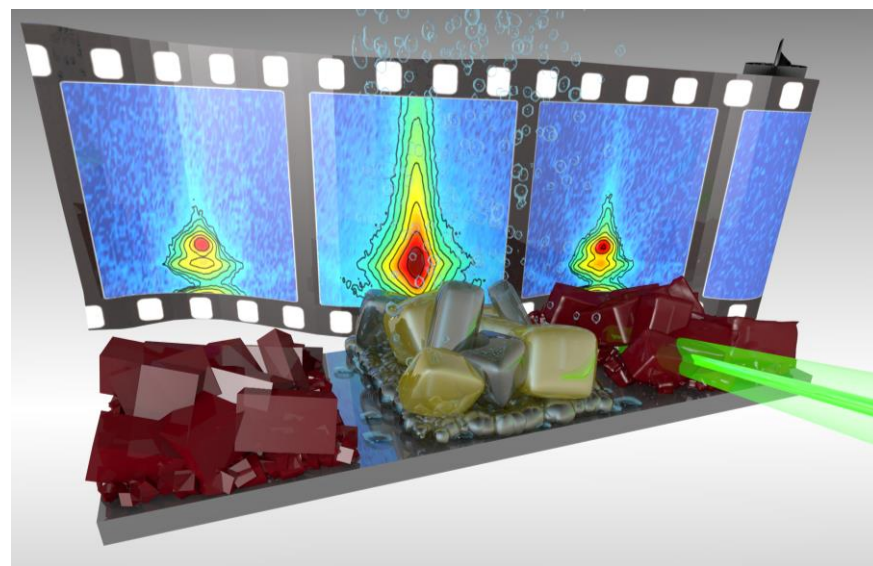
# Monitoring the Ingression of Moisture into Hybrid Perovskite Thin Films with In-Situ GISANS

Johannes Schlipf<sup>1</sup>,

L. Bießmann<sup>1</sup>, L. Oesinghaus<sup>2</sup>,

E. Berger<sup>3</sup>, E. Metwalli<sup>1</sup>, J. A. Lercher<sup>3</sup>,

L. Porcar<sup>4</sup>, P. Müller-Buschbaum<sup>1</sup>



1 Technische Universität München, Lehrstuhl für Funktionelle Materialien, Physik-Department, Garching (D)

2 Technische Universität München, Physics of Synthetic Biological Systems, Physics-Dept., Garching (D)

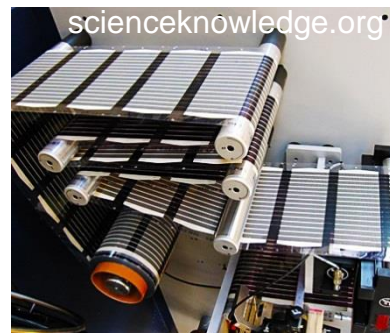
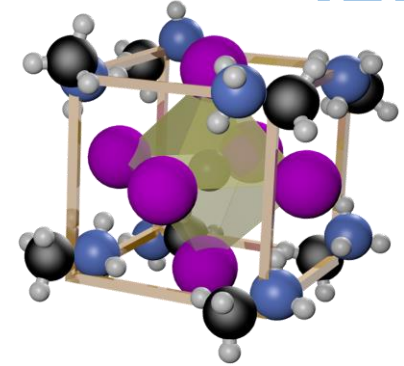
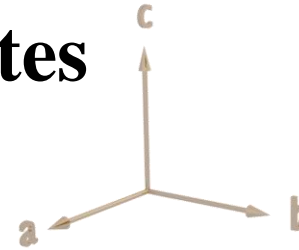
3 Technische Universität München, Department of Chemistry and Catalysis Research Center, Garching (D)

4 Institut Laue-Langevin (ILL), Beamline D22, Grenoble (F)

J. Schlipf et al., *J. Phys. Chem. Lett.* **2018**, 9, 2015

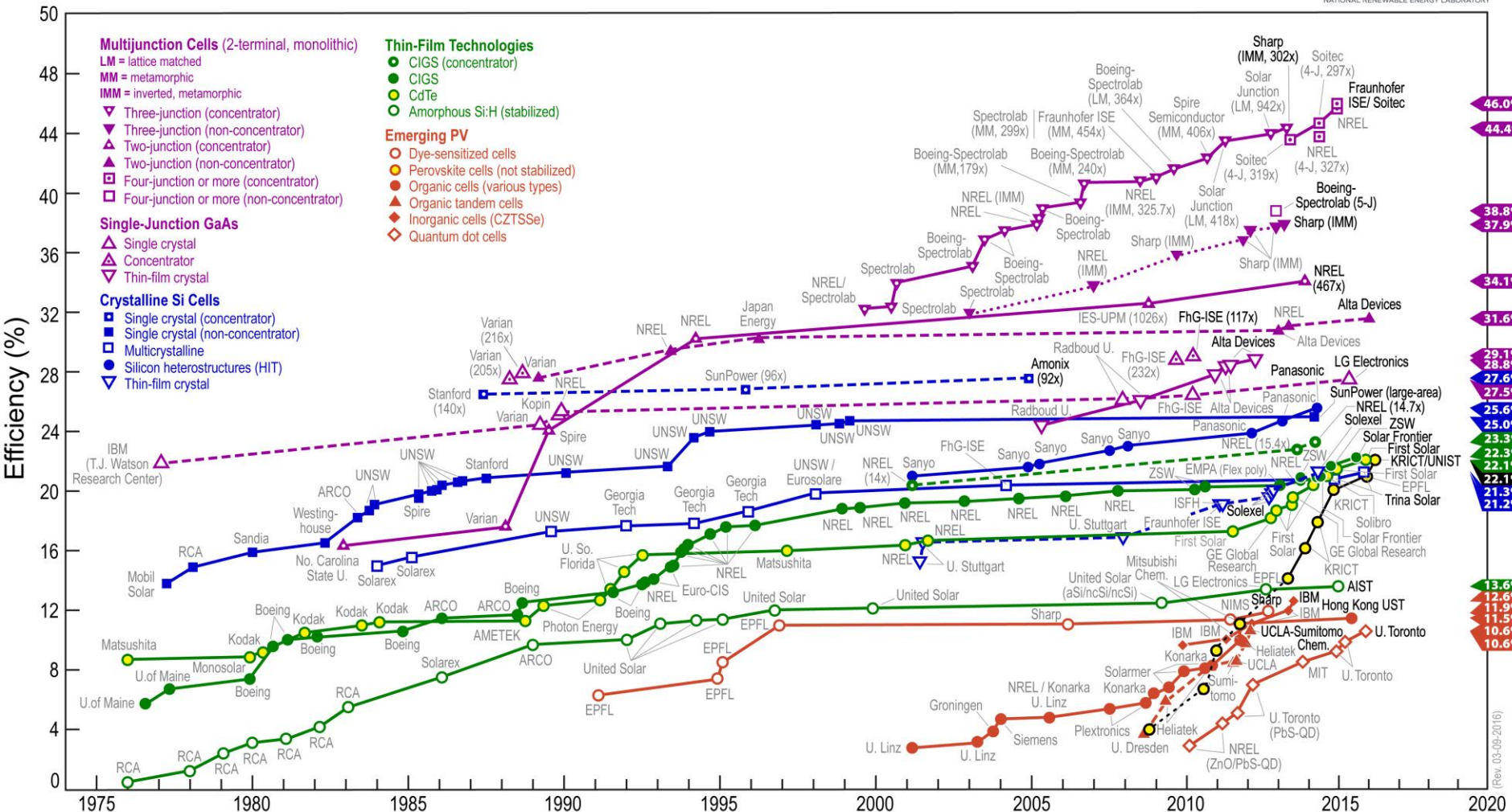
# Properties of hybrid perovskites

- ✓ exceptional optoelectronic properties
- ✓ photovoltaic efficiency > 20 %
- ✓ highly tunable by composition
- ✓ earth-abundant precursor materials
- ✓ solution processing
  - ➔ low production costs
- ✓ large-scale applicability
- ✓ device lifetimes
  - ≥ 1 year feasible<sup>[2]</sup>
- ✗ degradation with moisture

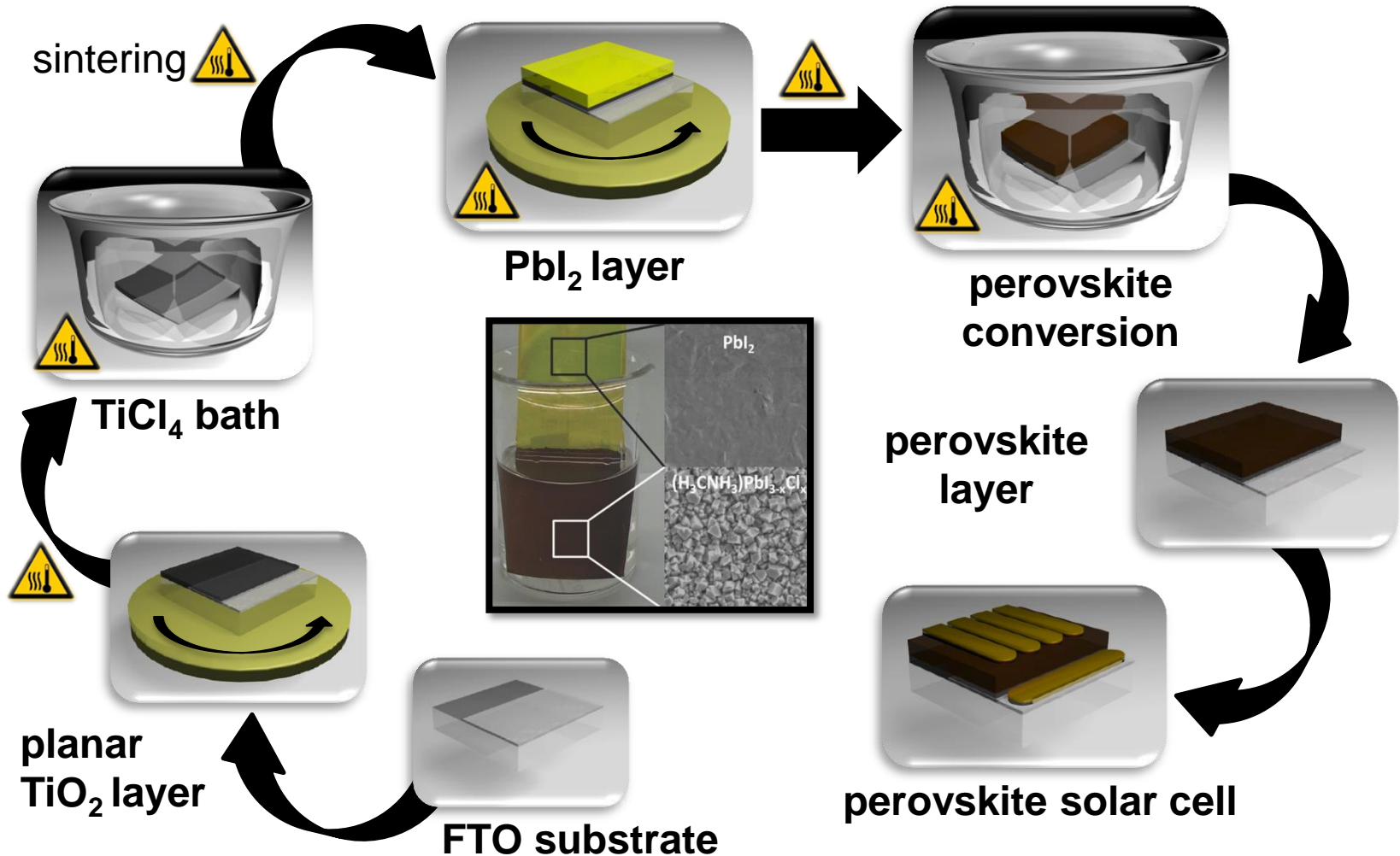




# Best research cell power conversion efficiencies



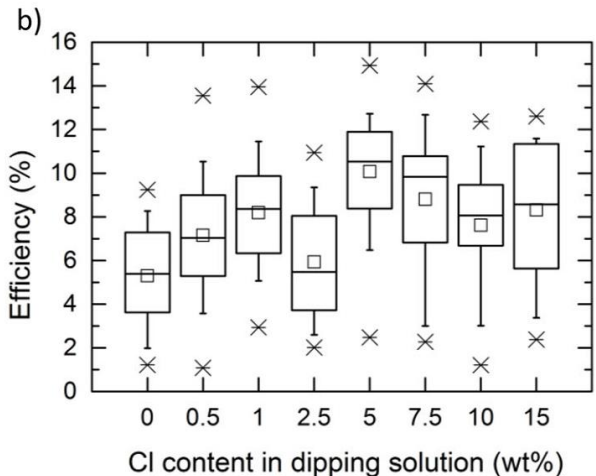
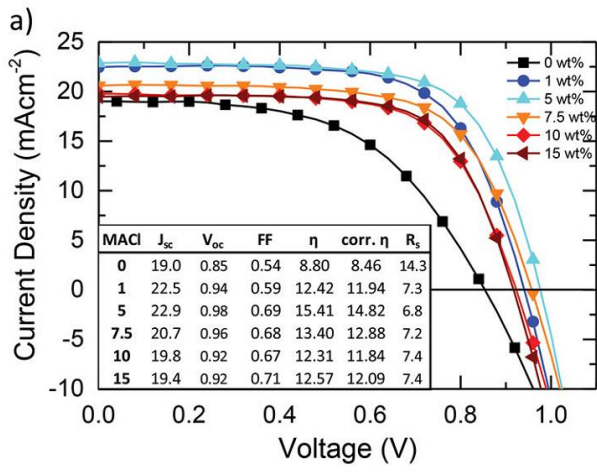
# Preparation of planar solar cells



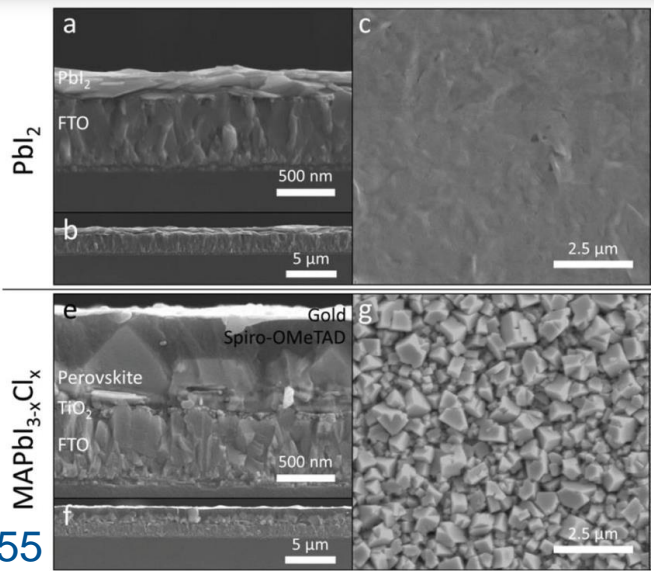
# Planar perovskite solar cells

**Solution Deposition-Conversion for Planar Heterojunction Mixed Halide Perovskite Solar Cells**  
 Pablo Docampo, Fabian C. Hanusch, Samuel D. Stranks, Markus Döblinger, Johann M. Feckl, Martin Ehrensperger, Norma K. Minar, Michael B. Johnston, Henry J. Snaith, and Thomas Bein

The alkylammonium metal trihalide perovskite absorbers first used in working photovoltaic devices were based on liquid electrolyte sensitized solar cells. Introduced by Kojima et al., the devices exhibited a starting point power conversion efficiency of 3.8% and, with further work, they were quickly improved to reach over 6%.<sup>[1]</sup> It was not until a solid-state configuration was employed, however, that high device efficiencies were achieved.<sup>[2]</sup> Initial results were reported at 9% for perovskite sensitized titanium-based devices<sup>[3]</sup> and further improvements were simultaneously achieved in a "meso-superstructured" configuration by replacing the mesoporous TiO<sub>2</sub> scaffold with an electronically inactive mesoporous Al<sub>2</sub>O<sub>3</sub> layer, exhibiting device efficiencies of over 12%.<sup>[4]</sup> Some of the key advantages for this material system over other competing device concepts are that they are compatible with low-temperature, solution-based processing and can be fully processed at low temperatures, thus making their use in flexible device applications.<sup>[4]</sup> Minar et al. have demonstrated a mesoporous perovskite film is deposited over a mesoporous TiO<sub>2</sub> scaffold fully converted into a second phase, a mixed halide perovskite, which exhibits a high device performance of 15.7% is currently the highest performance achieved for perovskite solar cells, pointing out the need for further technological improvements.<sup>[5]</sup> The short circuit currents demonstrated for the devices prepared by Liu and co-workers of over 20 mA cm<sup>-2</sup> are still short of the maximum current of over 25 mA cm<sup>-2</sup> reasonably achievable, taking into account other losses for this material.<sup>[6]</sup> A crucial limitation is the low diffusion length of around ~100 nm of the perovskite species in the MAPbI<sub>3</sub> perovskite.<sup>[6]</sup> This is greatly extended to over 1 μm with the inclusion of a precursor solution.<sup>[6]</sup> Furthermore, it is shown that the inclusion of chloride is beneficial to the photovoltaic performance.<sup>[6]</sup> It is expected that the incorporation of chloride will be transparent in the photoactive layer.<sup>[6]</sup> This is shown in the precursor solution.<sup>[6]</sup> The incorporation of chloride results in improved short-circuit current densities and in effect reduces the overall photovoltaic performance.<sup>[6]</sup> This is due to the incorporation of chloride into the perovskite structure, which leads to the near *in-situ* perovskite formation, which is a need for the extended diffusion length of the perovskite species.<sup>[6]</sup> This is a result of the interpenetration of nanometers, and in effect reduces the overall photovoltaic performance.<sup>[6]</sup>



- **method for highly efficient planar perovskite solar cells with PCE ~15 %**
- dense, compact and homogeneous films
- Cl additive influences film growth and PCE
- **nowadays basis for many 2-step synthesis methods = model system**

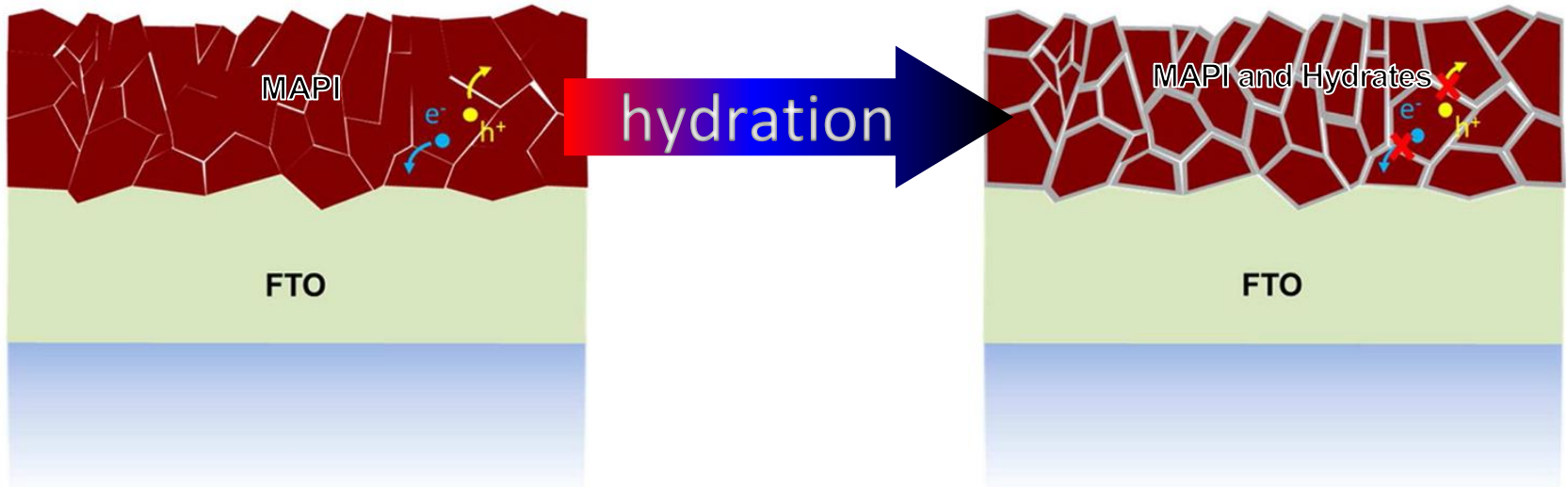
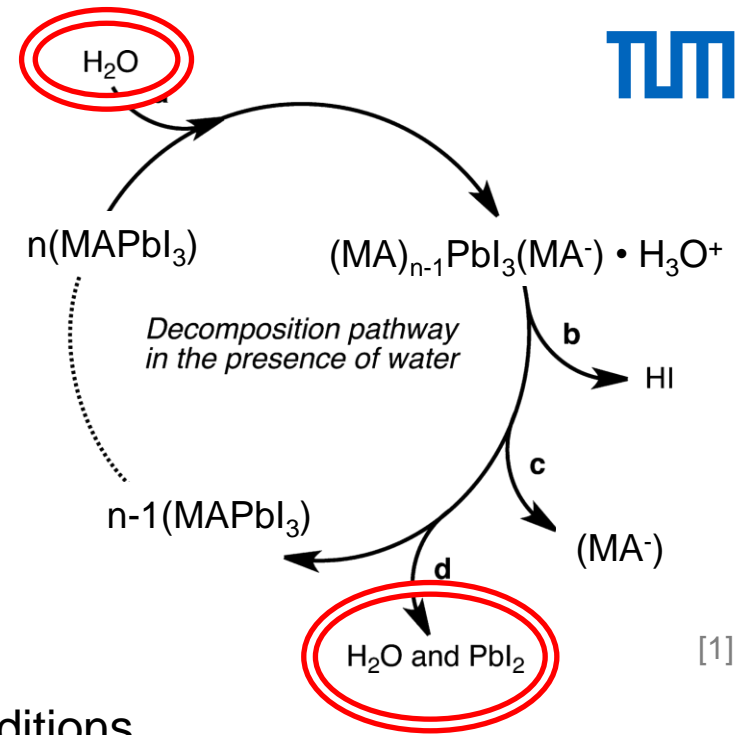


P. Docampo et al., *Adv. Energy Mater.* **2014**, *14*, 1400355



# Degradation with moisture

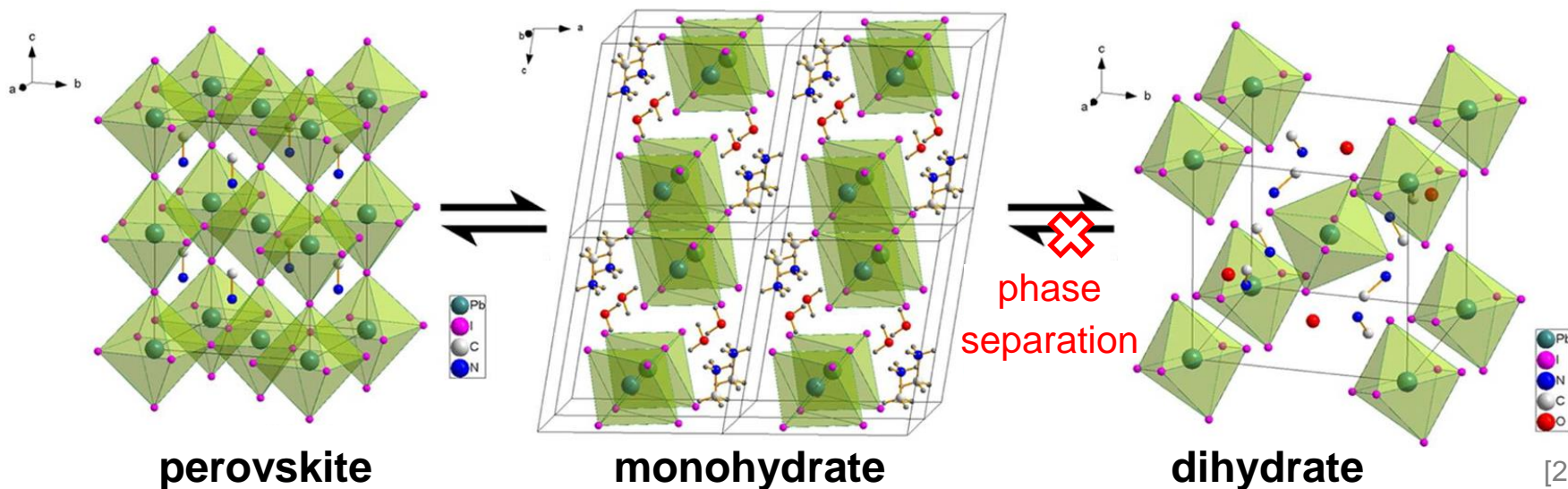
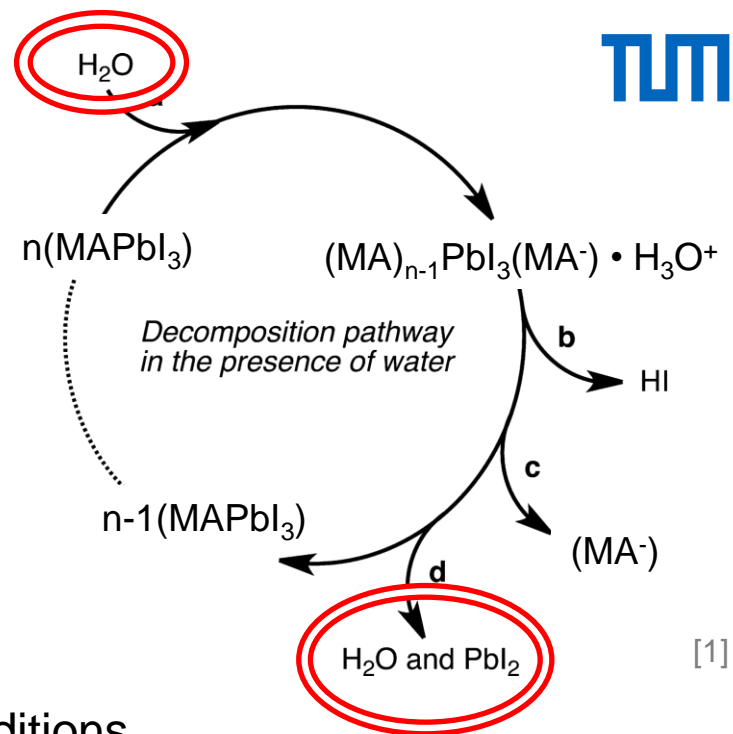
- high ambient humidity detrimental for photovoltaic performance
- degradation to  $\text{PbI}_2$  in self-sustaining reaction
- formation of metastable hydrate phases
- recovery of perovskite possible for certain conditions



[2]

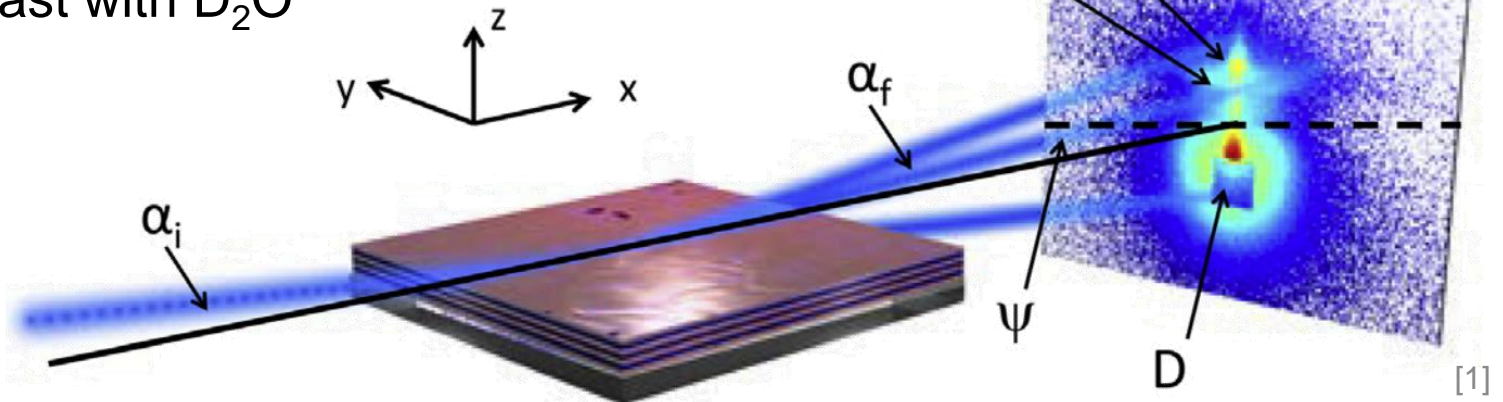
# Degradation with moisture

- high ambient humidity detrimental for photovoltaic performance
- degradation to  $\text{PbI}_2$  in self-sustaining reaction
- formation of metastable hydrate phases
- recovery of perovskite possible for certain conditions



# In-situ GISANS in humid atmosphere

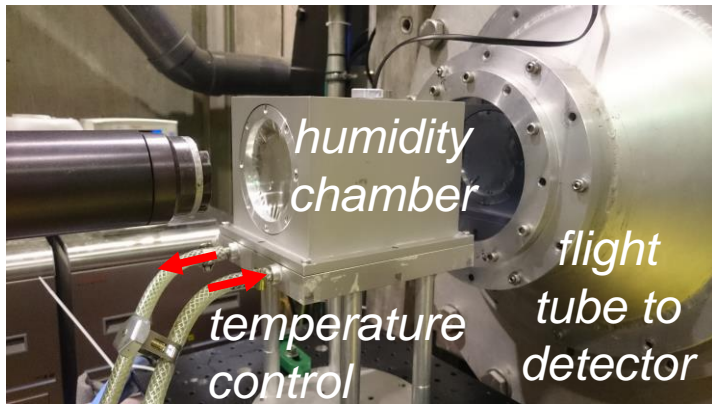
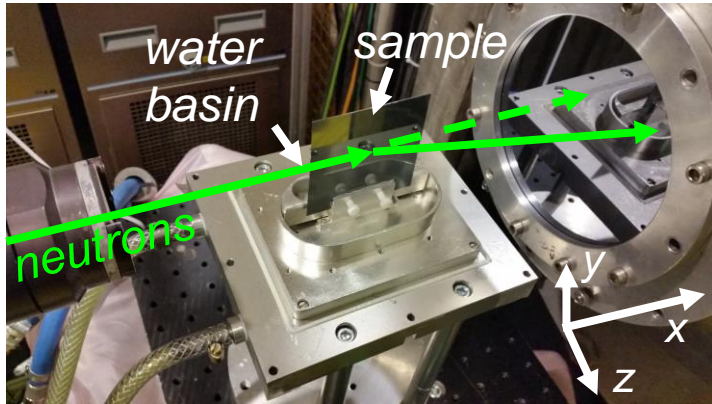
- ✓ non-destructive
- ✓ probing large sample volume  
→ high statistics
- ✓ high flux → 10 min/frame
- ✓ inner film morphology
- ✓ also non-crystalline material
- ✓ high contrast with  $D_2O$



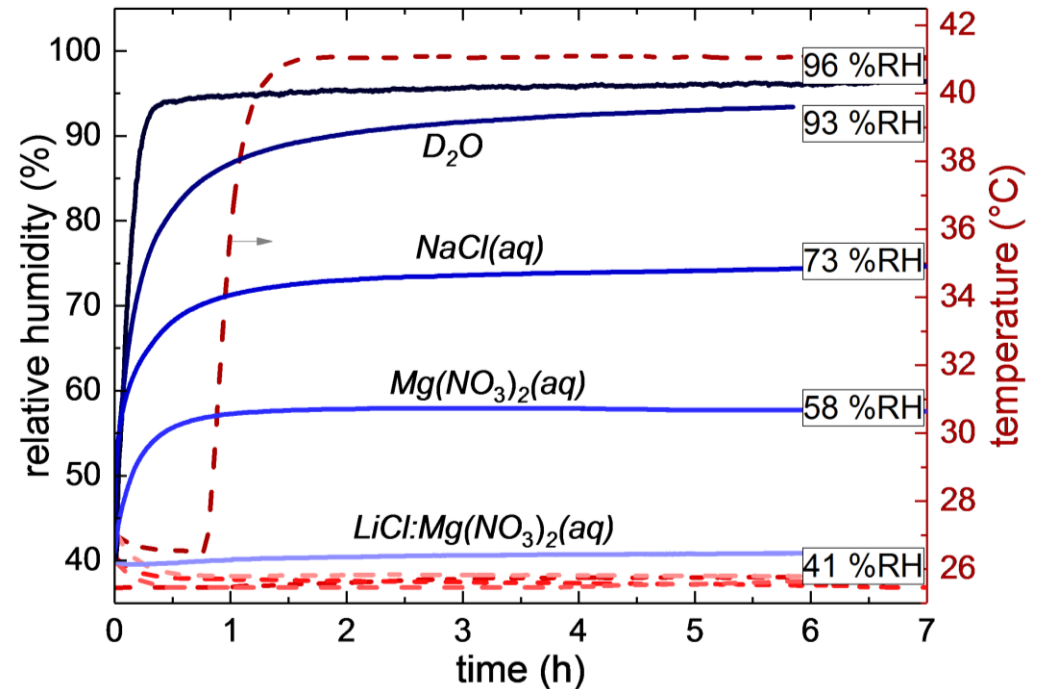
[1] P. Müller-Buschbaum, *Eur. Polym. J.* **2016**, 81, 470



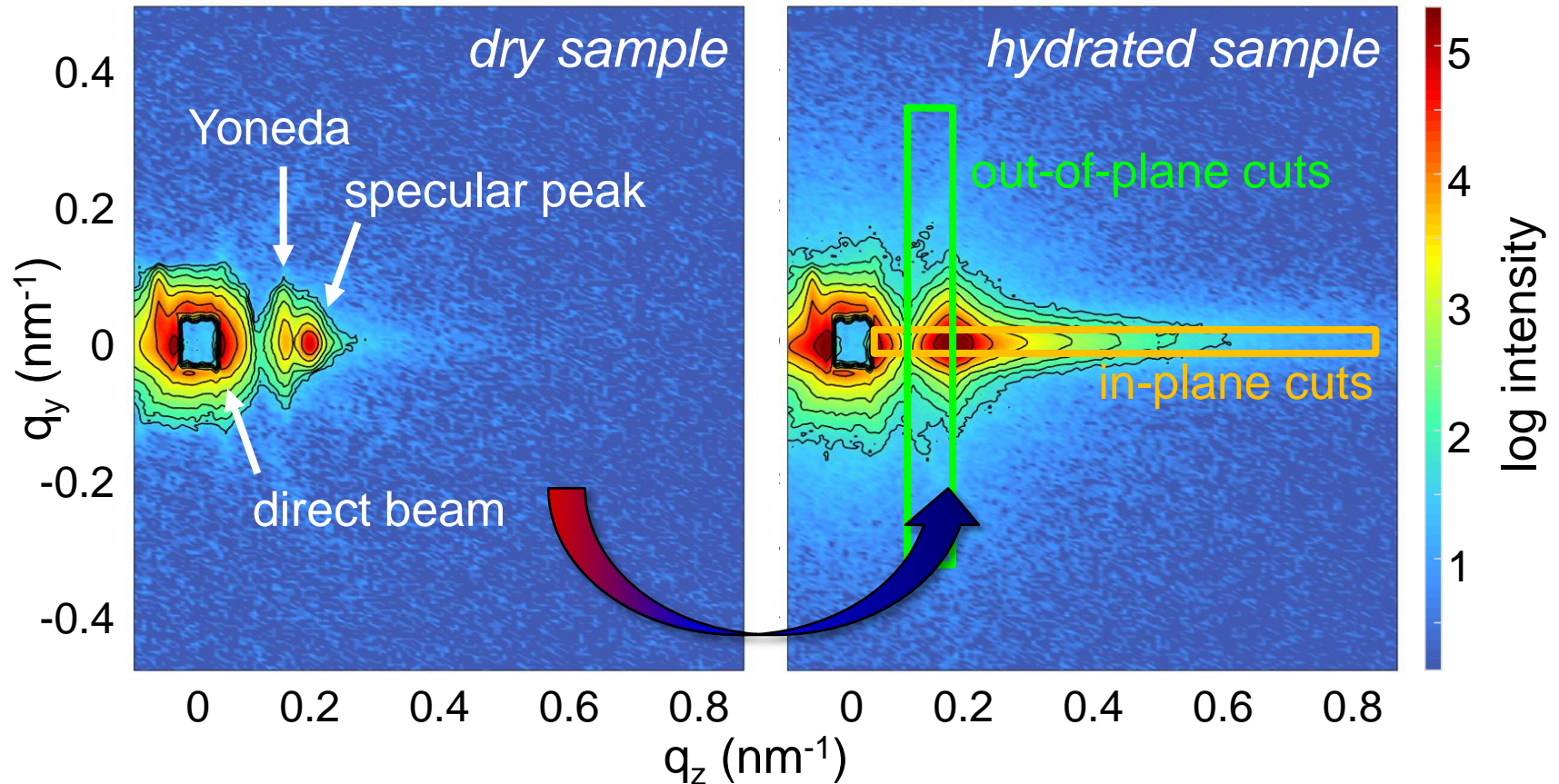
# In-situ GISANS – experiment design



- inject  $D_2O$  or salt solutions into chamber
- control temperature, monitor humidity



# In-situ GISANS – data acquisition and treatment



refractive index:  $n = 1 - \delta$

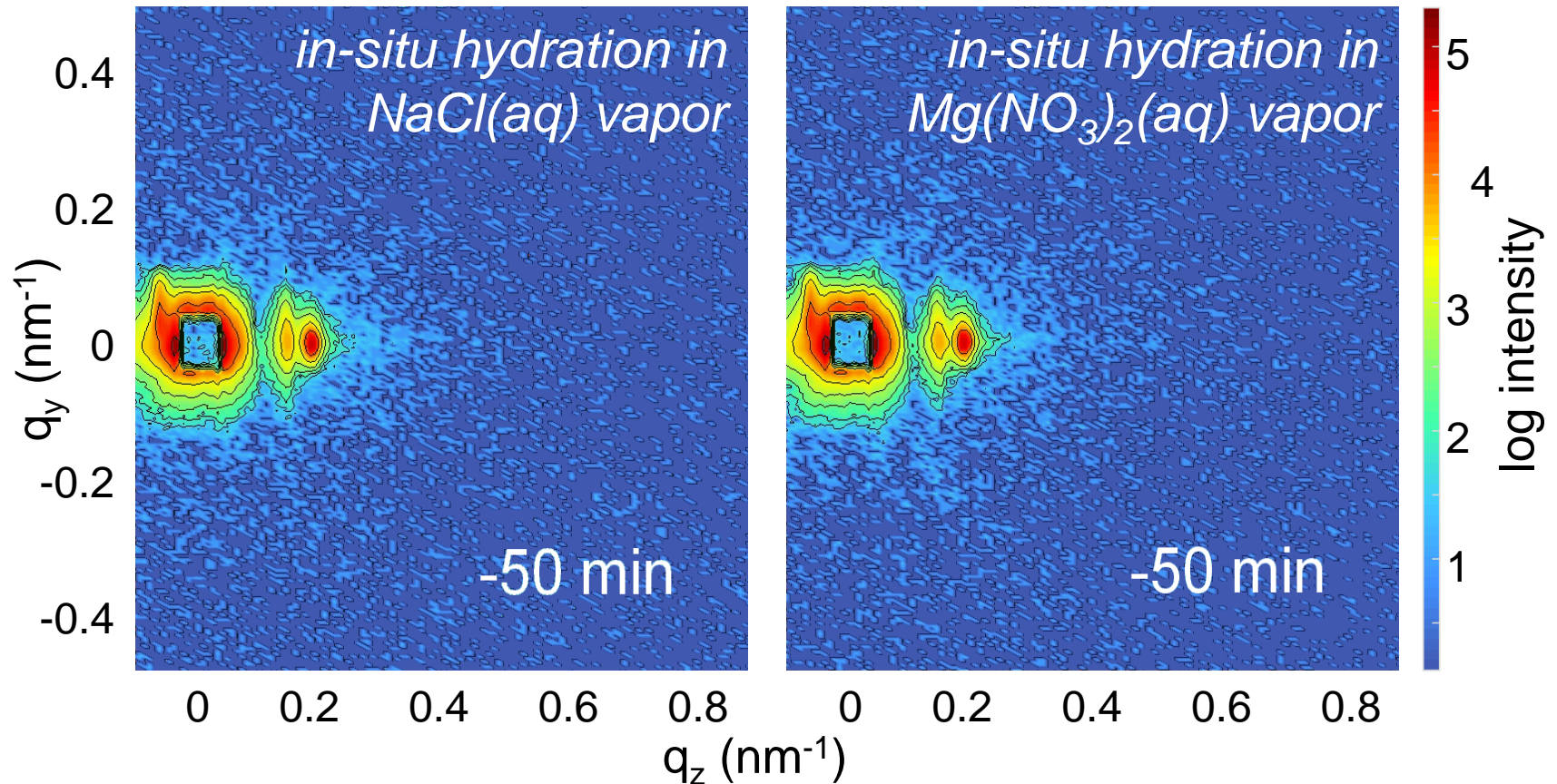
$\Rightarrow$  scattering length density:  $Nb = \frac{2\pi}{\lambda^2} \delta$

$\Rightarrow$  critical angle:  $\alpha_c = \lambda \sqrt{\frac{Nb}{\pi}}$

J. Schlipf et al., *J. Phys. Chem. Lett.* **2018**, 9, 2015



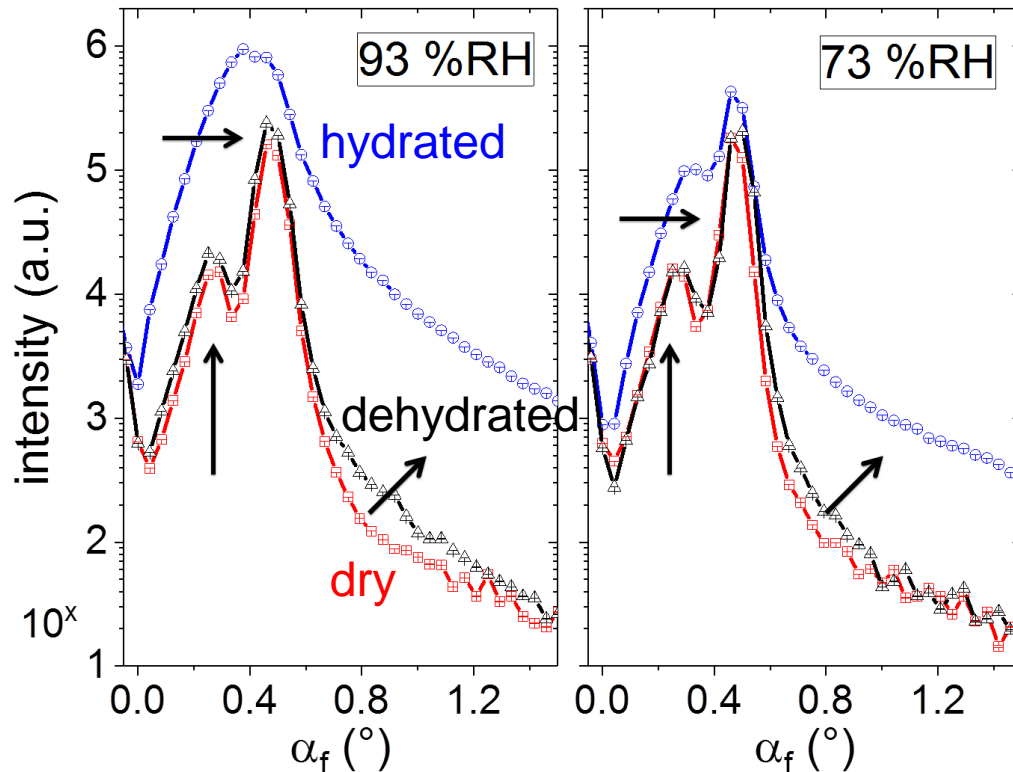
# In-situ GISANS – high vs. low humidity conditions





# Snapshots from the highest humidity levels

*in-plane cuts*

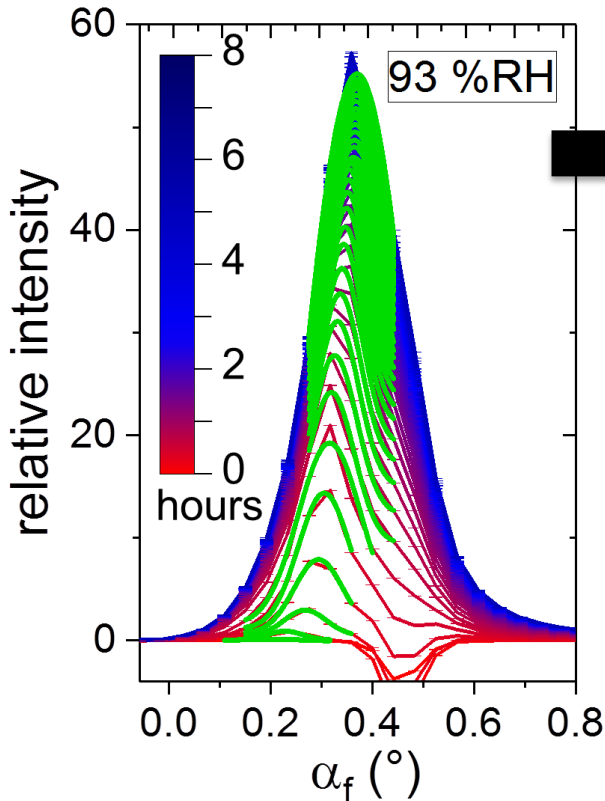


- strong shift of Yoneda peak for **hydrated** films
- higher roughness in dehydrated films than in **dry** ones
- $\text{PbI}_2$  formed for 93 %RH
- MAPI recovered for 73 %RH

➔ permanent morphological changes for high humidity levels

# Following water uptake in situ

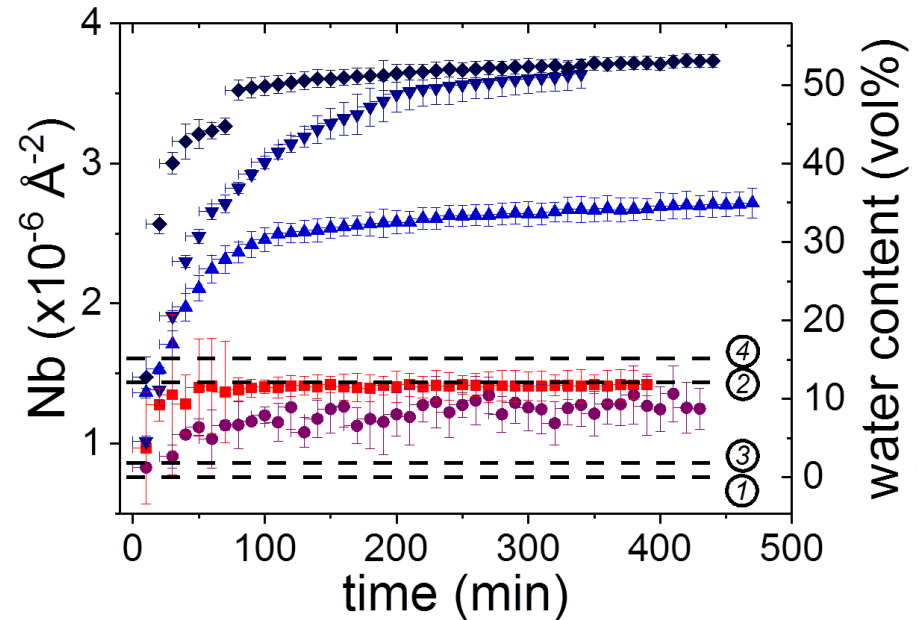
*in-plane cuts – 1<sup>st</sup> frame*



$$\alpha_c = \lambda \sqrt{\frac{Nb}{\pi}}$$

- 41 %RH
- 58 %RH
- ▲ 73 %RH
- ▼ 93 %RH
- ◆ 96 %RH

$$x \cdot Nb_{D_2O} + (1 - x) \cdot Nb_{MAPI} = Nb_{mix}$$

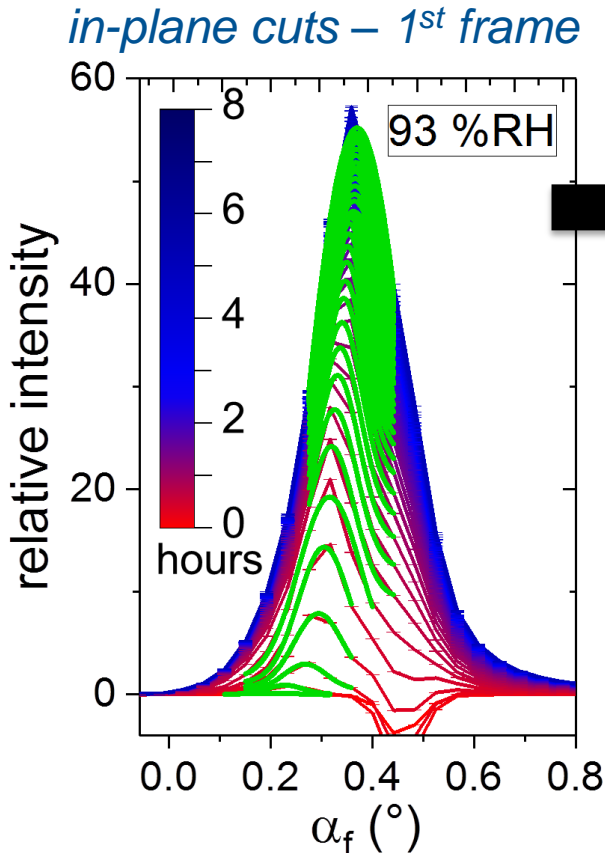


- up to 50 vol% water uptake
- 10 vol% water uptake for low humidity

- ① MAPI
- ② monohydrate
- ③ dihydrate
- ④  $PbI_2$

J. Schlipf et al., *J. Phys. Chem. Lett.* **2018**, 9, 2015

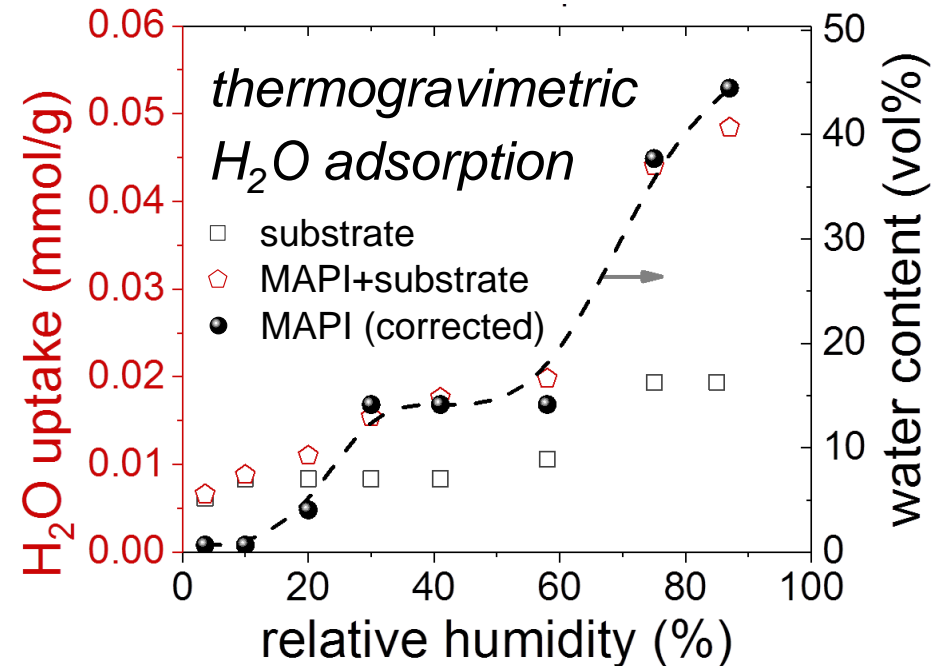
# Following water uptake in situ



$$\alpha_c = \lambda \sqrt{\frac{Nb}{\pi}}$$

- 41 %RH
- 58 %RH
- ▲ 73 %RH
- ▼ 93 %RH
- ◆ 96 %RH

$$x \cdot Nb_{D2O} + (1 - x) \cdot Nb_{MAPI} = Nb_{mix}$$



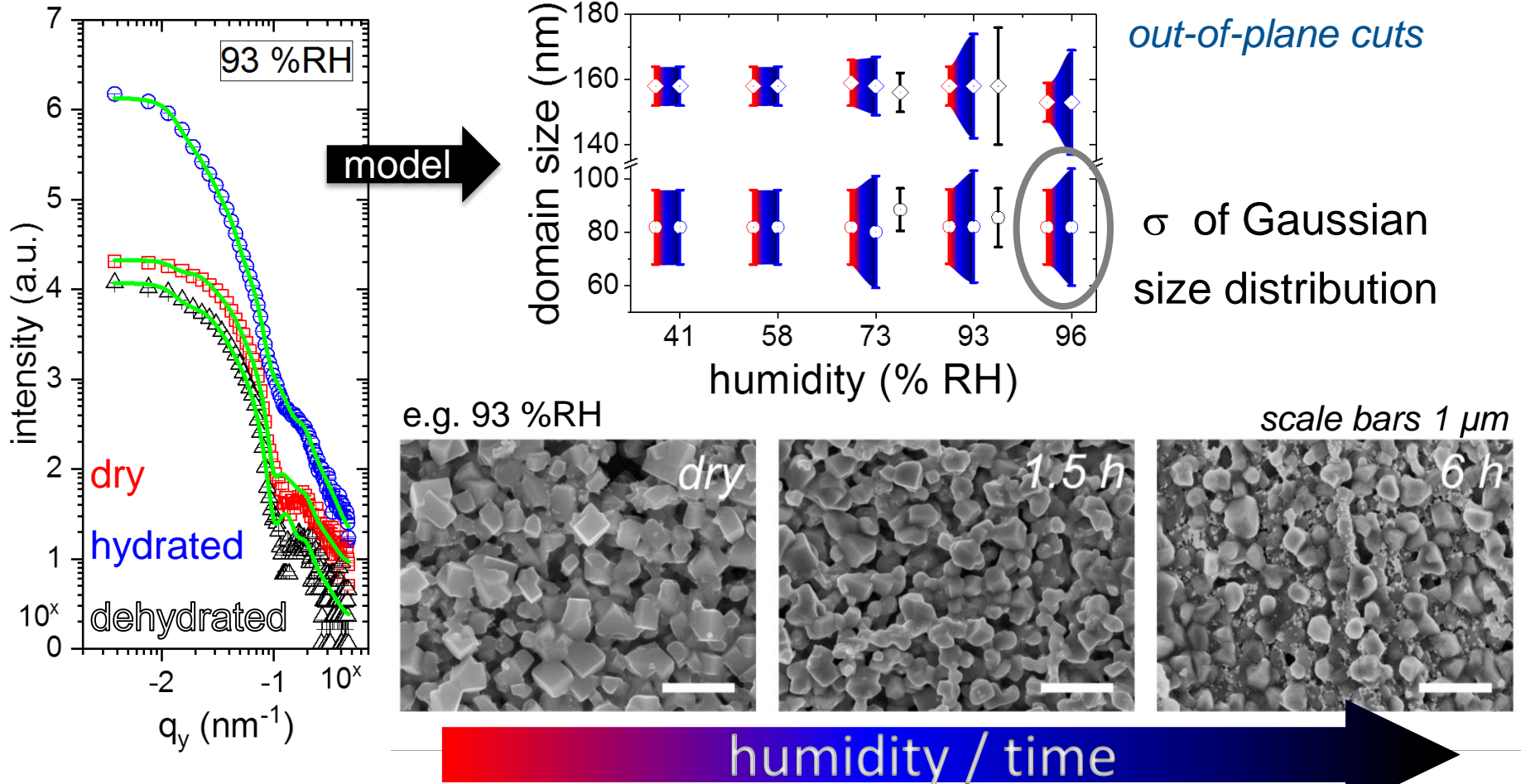
- ① MAPI
- ② monohydrate
- ③ dihydrate
- ④ PbI<sub>2</sub>

- up to 50 vol% water uptake
- 10 vol% water uptake for low humidity
- plateau → intermediate saturation level

J. Schlipf et al., *J. Phys. Chem. Lett.* **2018**, 9, 2015



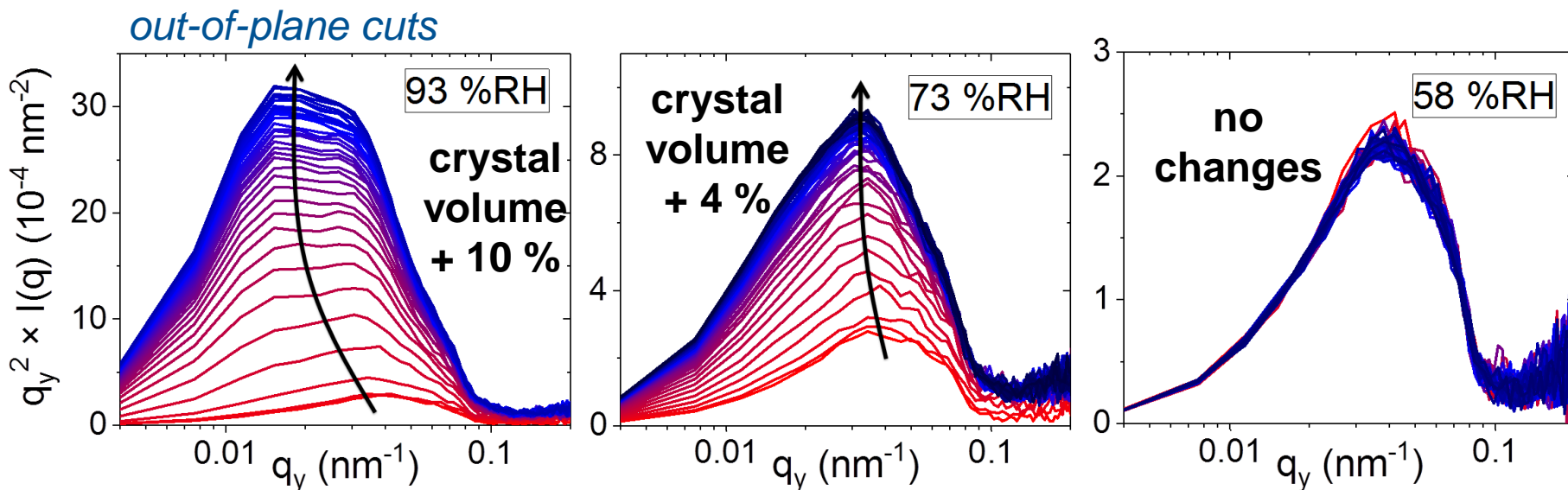
# Morphological changes due to hydration



→ domains become less defined for humidity levels  $\geq 73$  %RH

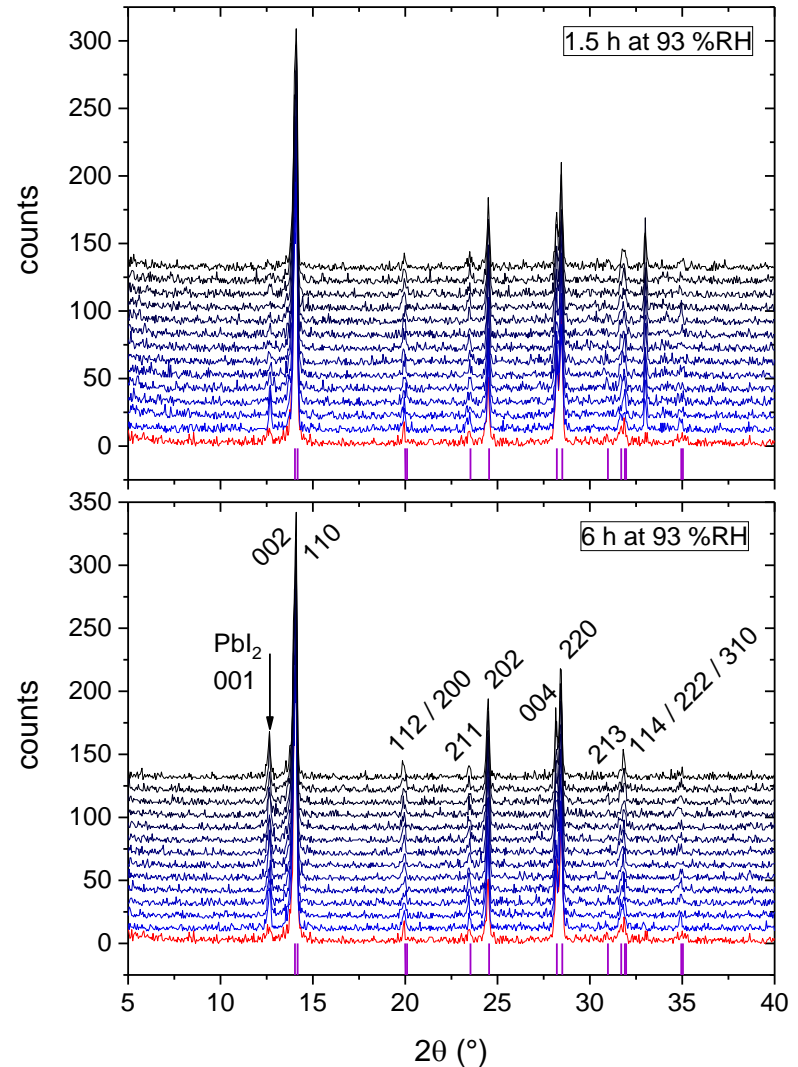
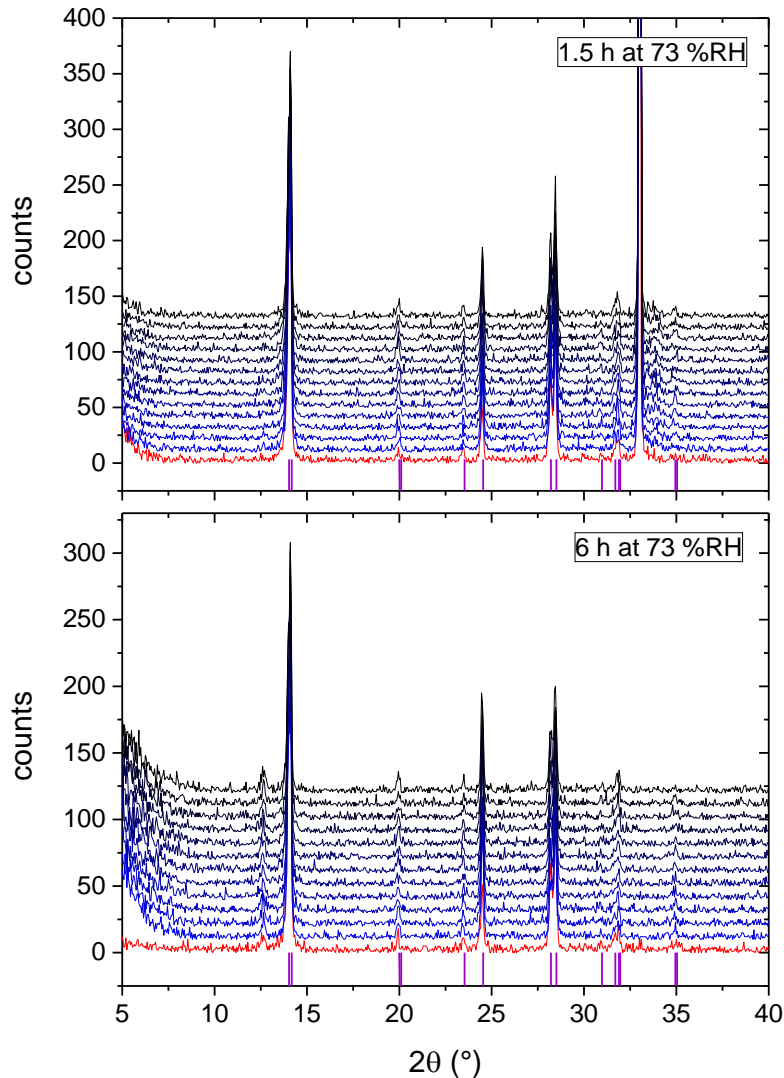
J. Schlipf et al., *J. Phys. Chem. Lett.* **2018**, 9, 2015

# Crystal inflation reveals composition



- Kratky representation reveals slight crystal inflation for first 1.5 h
- mostly monohydrate = MAPI volume + 7 % vs. dihydrate = MAPI  $\times$  250 %
- no apparent changes for humidity  $\leq$  58 %RH  $\rightarrow$  no monohydrate
- $\rightarrow$  water for low humidity not incorporated into crystals

# In-situ XRD during dehydration

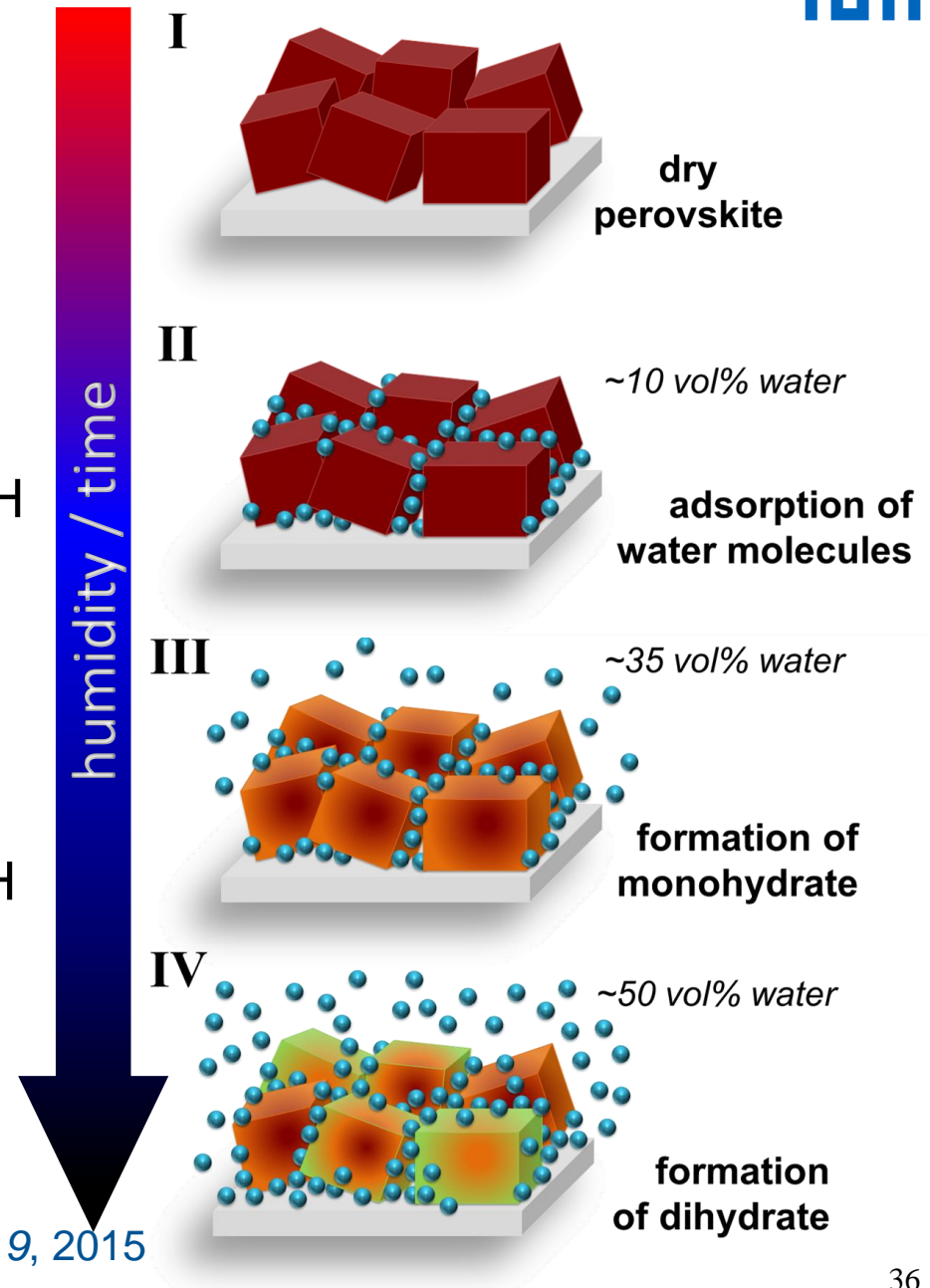




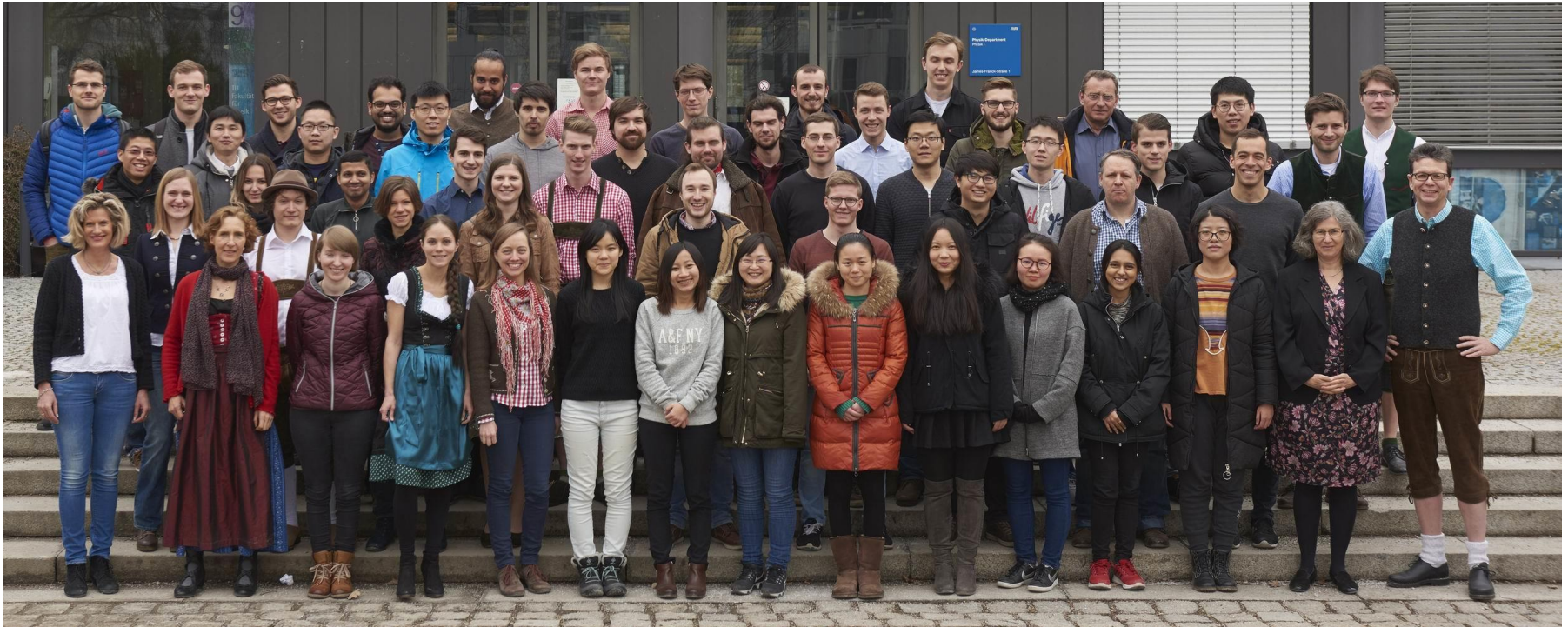
# Conclusions

- in-situ GISANS with high time resolution
- ingress of moisture at low %RH
  - level of monohydrate
  - no hydrates formed
  - most water adsorbed
- sponge-like behavior at high %RH
  - strong morphological changes of crystal domains for  $\geq 73$  %RH
  - formation of hydrates

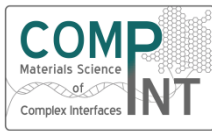
J. Schlipf et al., *J. Phys. Chem. Lett.* **2018**, 9, 2015



# Acknowledgments



Federal Ministry  
of Education  
and Research



Elitenetzwerk  
Bayern



SOLAR TECHNOLOGIES  
GO HYBRID

**TUM.solar**  
MS



IGSSE TUM  
International Graduate School  
of Science and Engineering



**DFG** Deutsche  
Forschungsgemeinschaft

EuroTech Universities



